NAVAL POSTGRADUATE SCHOOL
Monterey, California

THESIS

STUDY OF VORTEX ARRAYS INDUCED ARTIFICIALLY AND FROM CENTRIFUGAL INSTABILITIES

by

Michael F. Tuzzolo

June 1989

Thesis Advisor: Phillip M. Ligrani
Co-Advisor: Chelakara S. Subramanian

Approved for public release; distribution is unlimited

REPORT DOCUMENTATION PAGE

Form Approved
OMB No. 0704-0188

1a REPORT SECURITY CLASSIFICATION UNCLASSIFIED	1b RESTRICTIVE MARKINGS
2a SECURITY CLASSIFICATION AUTHORITY	3 DISTRIBUTION/AVAILABILITY OF REPORT Approved for public release; distribution is unlimited
2b DECLASSIFICATION/DOWNGRADING SCHEDULE	
4 PERFORMING ORGANIZATION REPORT NUMBER(S)	5 MONITORING ORGANIZATION REPORT NUMBER(S)
6a NAME OF PERFORMING ORGANIZATION Naval Postgraduate School 6b OFFICE SYMBOL (If applicable) Code 69	7a NAME OF MONITORING ORGANIZATION Naval Postgraduate School
6c ADDRESS (City, State, and ZIP Code) Monterey, California 93943-5000	7b ADDRESS (City, State, and ZIP Code) Monterey, California 93943-5000
8a NAME OF FUNDING/SPONSORING ORGANIZATION 8b OFFICE SYMBOL (If applicable)	9 PROCUREMENT INSTRUMENT IDENTIFICATION NUMBER
8c ADDRESS (City, State, and ZIP Code)	10 SOURCE OF FUNDING NUMBERS PROGRAM ELEMENT NO / PROJECT NO / TASK NO / WORK UNIT ACCESSION NO

11 TITLE (Include Security Classification)
STUDY OF VORTEX ARRAYS INDUCED ARTIFICIALLY AND FROM CENTRIFUGAL INSTABILITIES

12 PERSONAL AUTHOR(S)
Tuzzolo, Michael F.

13a TYPE OF REPORT	13b TIME COVERED	14 DATE OF REPORT (Year Month Day)	15 PAGE COUNT
Master's Thesis	FROM _____ TO _____	1989, June	95

16 SUPPLEMENTARY NOTATION
The views expressed in this thesis are those of the author and do not reflect the official policy or position of the Department of Defense or the U.S. Government.

17 COSATI CODES			18 SUBJECT TERMS (Continue on reverse if necessary and identify by block number)
FIELD	GROUP	SUB-GROUP	Embedded Vortices; Vortex Pairs, Vortex Arrays; Turbulent Boundary Layers, Dean Vortices, Centrigugal Instabilities; Laminar Flow

19 ABSTRACT (Continue on reverse if necessary and identify by block number)

Experimental results are presented which describe the development and structure of: (1) vortex pairs and vortex arrays which are embedded in turbulent boundary layers, and (3) vortex arrays developing as a result of centrifugal instabilities in a curved channel.

Streamwise vortex pairs embedded in a turbulent boundary layer on a flat plate are induced artificially using vortex generators. Mean velocity surveys, total pressure surveys, and wall heat transfer distributions show that Stanton numbers are augmented when vortex pairs have a common downwash. With common upwash, the Stanton number perturbation from vortex pairs is much less.

Vortex arrays induced from centrifugal instabilities were studied in a 40:1 aspect ratio channel with mild curvature. Mean velocity and total

20 DISTRIBUTION/AVAILABILITY OF ABSTRACT	21 ABSTRACT SECURITY CLASSIFICATION
☒ UNCLASSIFIED/UNLIMITED ☐ SAME AS RPT ☐ DTIC USERS	Unclassified
22a NAME OF RESPONSIBLE INDIVIDUAL Prof. Phillip M. Ligrani	22b TELEPHONE (Include Area Code) (408) 646-3382 22c OFFICE SYMBOL Code 69Li

DD Form 1473, JUN 86 *Previous editions are obsolete*

#19 - ABSTRACT - (CONTINUED)

pressure surveys for Dean numbers from 50 to 150 illustrate some structural characteristics of vortex pairs.

Approved for public release; distribution is unlimited

Study of Vortex Arrays Induced Artificially and From Centrifugal Instabilities

by

Michael F. Tuzzolo
Lieutenant, United States Navy
B.M.E., Villanova University, 1980

Submitted in partial fulfillment of the
requirements for the degree of

MASTER OF SCIENCE IN MECHANICAL ENGINEERING
And
MECHANICAL ENGINEER

from the

NAVAL POSTGRADUATE SCHOOL
June 1989

ABSTRACT

Experimental results are presented which describe the development and structure of: (1) vortex pairs and vortex arrays which are embedded in turbulent boundary layers, and (2) vortex arrays developing as a result of centrifugal instabilities in a curved channel.

Streamwise vortex pairs embedded in a turbulent boundary layer on a flat plate are induced artificially using vortex generators. Mean velocity surveys, total pressure surveys, and wall heat transfer distributions show that Stanton numbers are augmented when vortex pairs have a common downwash. With common upwash, the Stanton number perturbation from vortex pairs is much less.

Vortex arrays induced from centrifugal instabilities were studied in a 40:1 aspect ratio channel with mild curvature. Mean velocity and total pressure surveys for Dean numbers from 50 to 150 illustrate some structural characteristics of vortex pairs.

TABLE OF CONTENTS

LIST OF TABLES

LIST OF FIGURES

NOMENCLATURE

Symbol	Name	Units
A	Area	m^2
x,X	Freestream Length	m
y,Y	Vertical Length	m
z,Z	Spanwise Length	m
b	Distance Between Vortex Generates Base Midpoints	m
U_∞	Freestream Mean Velocity	m/s
U_x	Streamwise Mean Velocity Component	m/s
U_y, U_z	y,z Mean Velocity Components	m/s
R	Gas Constant (Air)	J/kg·k
c_p	Constant Pressure Specific Heat (Air)	J/kg·k
λ_F	Freestream Recovery Factor	
λ_{BL}	Boundary Layer Recovery Factor	
P_∞	Freestream Pressure	Pa or mm
P_{stat}	Static Pressure	Hg or H_2O
Po_∞	Freestream Stagnation Pressure	Pa
P_{amb}	Ambient Pressure	Pa
P_{tot}	Total Pressure	Pa
T_∞	Freestream Temperature	^oC
Tr_∞	Boundary Layer Recovery	^oC

Tr_F	Freestream Recovery Temperature	^oC
T_{amb}	Ambient Temperature	^oC
ρ_x	Freestream Density	Kg/m^3
ρ_{amb}	Ambient Density	Kg/m^3
ν	Kinematic Viscosity	m^2/s
$\dot{q}_w$	Convective Heat Transfer Rate from Wall to Freestream	W
St	Stanton Number	(Dimensionless)
St_o	Stanton Number Baseline Values	(Dimensionless)
Re_x	Reynolds Number	(Dimensionless)
ω_x	Streamwise Vorticity	s^{-1}
α	Pitch Angle of 5-hole Probe	degrees
β	Yaw Angle of 5-hole Probe	degrees
V_T	Total Velocity	m/s
$P_1, P_2, P_3, P_4, P_5, P$	5-hole Probe Pressures	in H_2O
$C_{py}, C_{pp}, C_{pt}, C_{pts}$	5-hole Probe Calibration Coefficients	
K_p, K_y	5-hole Probe Calibration Curve Slope for Pitch and Yaw Angles	

FORMULAE

$$U_\infty = \left[\frac{2(P_{O\infty} - P_\infty)}{\rho_{amb}} \right]^{1/2}$$

$$\rho = \frac{P}{RT}$$

$$T_\infty = Tr_{\infty_F} - \frac{\alpha_F U_\infty^2}{2c_p}$$

$$Tr_\infty = T_\infty + \frac{\alpha_{BL} U_\infty^2}{2c_p}$$

$$St = \frac{\dot{q}_W}{A(T_W - Tr_\infty)\rho_\infty U_\infty C_p}$$

$$\omega_x = \frac{\partial U_z}{\partial y} - \frac{\partial U_y}{\partial z}$$

$$V_T = [U_x^2 + U_y^2 + U_z^2]^{1/2} = [2\, c_{pts}(P_1 - \bar{P})/\rho]^{1/2}$$

$$U_x = V_T \cos(\alpha)\cos(\beta)$$

$$U_y = V_T \sin(\alpha)$$

$$U_z = V_T \cos(\alpha)\sin(\beta)$$

$$C_{py} = (P_2 - P_3)/(P_1 - \bar{P})$$

$$C_{pp} = (P_4 - P_5)/(P_1 - \bar{P})$$

$$C_{pt} = (P_1 - P_{tot})/(P_1 - \bar{P})$$

$$C_{pts} = (\bar{P} - P_{stat})/(P_1 - \bar{P})$$

$$\bar{P} = (P_2 + P_3 + P_4 + P_5)/4$$

$$Re_x = \frac{U_\infty x}{\nu}$$

I. INTRODUCTION

A. APPLICATION

Streamwise embedded vortices are one type of secondary flow found in tubomachines. Such vortices are important because their intense secondary flows often lead to local hot spots.

Within turbine blade passages, vortices result from at least two different mechanisms, Ligrani et al. [Ref. 1]. First, they develop from intense local pressure gradients, such as the one formed at the intersection of the blade leading edge and endwall. Here, pressure forces the flow towards the endwall where it then rolls into the leading edge or horseshoe vortex. The horseshoe vortex then splits into a suction side leg and a pressure side leg. As the pressure side leg convects between blades, it is called the passage vortex. The second mechanism occurs near concave surfaces of turbine blades. Here, centrifugal instabilities cause faster moving fluid to move towards the wall to displace slower moving fluid in the boundary layer. The resulting spanwise varying regions of high and low speed flow form into Taylor-Goertler roll cells or vortices. These Taylor-Goertler structures most often develop as an array. Vortices which develop from intense local pressure gradients also often occur in pairs or groups.

The present study is intended to provide additional understanding of the behavior and effects of vortex pairs and vortex arrays particularly in regard to their influences on local heat transfer distributions.

B. RELATED STUDIES

Studies of the heat transfer effects of embedded vortices are relatively scarce. Eibeck and Eaton [Ref. 2] showed how embedded vortices caused Stanton number increases as great as 24 percent and decreases of 14 percent in flat plate turbulent boundary layers. The variations in heat transfer were found to increase with the circulation of the vortices. In addition, they were found to persist along the entire length of their test section, which was over 100 initial boundary layer thicknesses long. Effects of embedded longitudinal vortices on heat transfer in film-cooled boundary layers have been studied by Ligrani et al. [Refs. 1,3], Ligrani and Williams [Ref. 4], and Craig [Ref. 5].

C. OBJECTIVES OF PRESENT STUDY

The objectives of the present study are to measure and study the development and structure of: (1) vortex pairs and vortex arrays induced artificially in turbulent boundary layers, and (2) vortex arrays induced from centrifugal instabilities in a curved channel with laminar flow. For the former case, surface heat transfer distributions were

measured along with surveys of mean velocity components. For the latter case, surveys of mean total pressure and streamwise velocity were measured and studied.

D. THESIS ORGANIZATION

Thesis organization is as follows. Experimental apparatus and procedures are discussed in Chapter II. Vortex pair and vortex array data for the turbulent boundary layer portion of the study are given in Chapter III. Chapter IV presents measurements of vortex characteristics made in the curved channel with laminar flow. Chapter V gives a summary and conclusions. All figures referenced in the text of the thesis are found in Appendix A. The uncertainty levels for parameters measured and calculated in this study are tabulated in Appendix B.

II. EXPERIMENTAL APPARATUS AND PROCEDURES

A. WIND TUNNEL AND COORDINATE SYSTEM

The experiments were conducted in an open-circuit, subsonic wind tunnel located in the laboratories of the Department of Mechanical Engineering of the Naval Postgraduate School. A centrifugal blower was located at the upstream end of the tunnel. Air entered the inlet from the surrounding room through a coarse filter. The discharge from the fan passed to the inlet of the diffuser. A 1.6 mm clearance between fan and diffuser isolated vibrations from the fan to the wind tunnel body. The diffuser contained a second fine filter to remove small particles from the air as well as four baffle vanes to reduce noise and minimize the likelihood of flow separations. The diffuser was followed by a header containing a honeycomb and three screens to reduce spatial nonuniformities in the flow. A 16:1 contraction ratio nozzle led from the header to the test section. The test section was a rectangular duct 3.05 m long and 0.061 m wide. The height of the topwall was adjustable to permit changes in the streamwise pressure gradient. For the pressure study, a zero pressure gradient was maintained without vortex or film cooling to within 0.018 cm of water differential pressure along the length of

the test section. The air speed through the test section was adjustable from 1 m/s to 40 m/s.

At the exit plane of the nozzle, the variation of total pressure was less than 0.4 percent at 26 and 34 m/s. Mean velocity varied less than 0.7 percent for the same speeds. Profile measurements of the mean velocity and longitudinal turbulence intensity in the turbulent boundary layer developing at 20 m/s indicated normal, spanwise uniform behavior. At x = 1.8 m, measurements from hot-wire probes showed that the boundary layer thickness, boundary layer displacement thickness, and boundary layer momentum thickness were 29.7, 5.09, and 3.59 mm, respectively. At a freestream velocity of 21.0 m/s, the momentum thickness Reynolds number was 4780 and the friction velocity was 0.8 m/s. The freestream turbulence intensity was about 0.1 percent (based on freestream velocity) for freestream velocities of 20-30 m/s. For this qualification test and the present study, the boundary layer was tripped near the exit of the nozzle with a 1.5 mm high strip of tape.

The coordinate system is shown in Figure 1. With the heat transfer surface at elevated temperature, an unheated starting length of 1.10 m existed. Freestream air was maintained at ambient temperature, and thus the direction of heat transfer was from the wall to the gas. With heat transfer, temperature differences were maintained less than about 30^{o}C to minimize the effects of variable properties.

Referring again to Figure 1, the leading edge of the vortex generator was placed 0.48 m downstream of the trip. Also labeled in Figure 1 are the locations of thermocouple rows along the test surface.

B. VORTEX GENERATORS

The vortex generator consisted of a half-delta wing attached to a 1/16 inch thick Lexan mounting plate. This device is attached to the wind tunnel floor so that the generator is at an angle of 15^{o} with respect to the tunnel center line. The generator design was similar to ones employed by Westphal et al. [Refs. 6,7] and by Eibeck and Eaton [Ref. 2]. The height of the delta wing was 3.0 cm, and the base was 7.5 cm as shown in Figure 2.

1. Vortex Pairs

A vortex pair was created when two vortex generators were positioned together as depicted in Figure 3.a and 3.b. A vortex downwash was created when the forward edge of each vortex generator was positioned 15^{o} with respect to the tunnel center line away from each other as shown in Figure 3.a. The opposite effect of a vortex upwash was created when the forward edge of each vortex generator was positioned 15^{o} with respect to the tunnel center line towards each other as shown in Figure 3.b. The distance between the two vortex generator base midpoints, b, was the parameter varied for testing. The distances used were 2.54, 3.81, 5.08, 6.35 and 7.62 cm.

2. Vortex Arrays

The combination of three vortex generator pairs attached to a 1/16 inch Lexan mounting plate resulted in the formation of a vortex array, as depicted in Figure 4. The space between each vortex generator pair centerline was held constant at 6.35 cm. The parameter b, values for each vortex generator pair were 3.71, 5.08 and 6.35 cm in the downwash configuration. The vortex generator array with an upwash configuration, had the parameter b = 6.35 cm.

C. HEAT TRANSFER MEASUREMENTS

The heat transfer surface was designed and developed to provide a constant heat flux over its area. The plate was constructed so that its upward-facing part was adjacent to the wind tunnel air stream, with minimal heat loss by conduction from the sides and beneath the test surface. The design was based on ones used at the University of Minnesota [Refs. 8,9]. It consisted of a thin stainless steel foil, 1.3 m x 0.467 m x 0.20 mm, painted flat black. Seven layers of liquid crystals were applied on top of the paint. Attached to the underside of the foil were 126 copper-constantan thermocouples in six rows. In each of the six rows, 21 thermocouples were located 1.27 cm apart to provide adequate spanwise resolution of temperature distributions. Thermocouple lead wires were located in grooves cut into a triple sheet of 0.254 mm thick double-sided tape (3M Company). The groves were then filled with epoxy. A thin

foil heater (Electrofilm Corp.), 1.0 mm x 1.118 m x 0.438 m and rated at 120 V and 1500 W, was attached to the tape with Electrobond epoxy. Beneath the heater was a 12.7 mm thick Lexan sheet, followed by 25.4 mm of foam insulation, 82.55 mm thick styrofoam, three sheets of 0.254 mm thick Lexan, and one sheet of 9.53 mm thick balsa wood. Additional details are given by Ortiz [Ref. 10].

The vertical height of the surface was adjustable to allow for thermal expansion. It was maintained level with the test surface by adjusting screws in the plexiglas frame supporting the heat transfer surface from below. During heat transfer tests, the top surface of the foil remained flat and smooth with minimal surface irregularities. The surface temperature was controlled by adjusting input voltage to the heater using a Standard Electrical Co. variac, type 3000B.

To qualify the heat transfer surface, a video system (Hughes Probeye Thermal Series 4000) consisting of an infrared and video camera with display screen was used to measure surface temperatures during tests with both forced and natural convection from the surface. Results showed that 90-95 percent of the heat transfer surface had spanwise uniform temperatures within a fraction of a degree celsius. The only exceptions were several small cool spots with temperatures about $1^{o}C$ lower than the rest of the plate.

Additional confirmation of the temperature uniformity of the surface was obtained using the liquid crystals.

To determine the heat loss by conduction from the heat transfer test surface, energy balance was performed. Radiation losses from the top of the test plate were estimated analytically. For an average plate temperature of 40°C with a free-stream of 10 m/s and 18°C, radiation losses were approximately 55 W, or about 8.5 percent of the total power into the test plate. The thermal contact resistance between thermocouples and the foil top surface was estimated on the basis of outputs of the thermocouples and measurements from calibrated liquid crystals on the surface of the foil. This difference was then correlated as a function of heat flux through the foil. Ortiz [Ref. 10] and Joseph [Ref. 11] give additional details.

D. TEMPERATURE MEASUREMENTS

The copper-constantan thermocouples were used to measure surface temperatures on the constant flux surface. They were calibrated using a temperature-regulated bath consisting of liquid nitrogen and electric heaters and a platinum resistance temperature gauge as a standard. Calibrations were performed over a temperature range of 0-45°C, and second-order polynomials were used to convert voltages to temperature. For plate temperatures, one calibration was used for all thermocouples of similar

manufacture, since their outputs were the same within 1-2 μV at any given temperature.

Voltages from the thermocouples were read by an HP-3497A data acquisition/control unit with an HP-3498A extender. These units were controlled by a Hewlett-Packard Series 300 Model 9836S computer equipped with an MC68000, 8 MHz 16/32-bit processor, dual 5 1/4 inch floppy disk drives, and 1 mega-byte of memory.

E. MEAN VELOCITY MEASUREMENTS

The three main-velocity components were measured using a five-hole pressure probe (United Sensors and Control Corporation). The probe was a conical type with a diameter of 0.635 cm. It was calibrated over a range of yaw angles from -40° to $+40^{\circ}$ and over a range of pitch and angles from -15° to $+15^{\circ}$. Data from the probe were corrected for the effects of spatial resolution using the procedures of Ligrani et al. [Ref. 1]. The probe was connected to five differential pressure transducers (Celesco Model LCVR), each with a range of 20 cm water differential pressure. Transducer output signals were converted to dc signals by Celesco CD-100 carrier demodulators, which were then connected to the same data-acquisition system that was used for temperature measurement. Additional details are given by Williams [Ref. 12] and Craig [Ref. 5].

III. EXPERIMENTAL RESULTS

The experimental results of this study are presented in the following order: (1) baseline heat transfer measurements, (2) heat transfer measurements and fluid mechanic measurements for vortex pairs, and (3) heat transfer measurements and fluid mechanic measurements for vortex arrays.

A. BASELINE HEAT TRANSFER MEASUREMENT RESULTS

1. Baseline Stanton Number Measurements without an Embedded Vortex

Baseline Stanton numbers are now discussed for the open circuit, subsonic wind tunnel with a turbulent boundary layer. Baseline Stanton numbers are spanwise averaged for each of the six rows of thermocouples. The contact resistance of the 126 thermocouples can deviate slightly from the values experimentally determined in Section II.C. To minimize the effect of these variations the results for local conditions are presented in terms of Stanton number ratios. The local Stanton number values are normalized using local baseline Stanton numbers. Several surveys were conducted to measure the baseline Stanton numbers without an embedded vortex positioned in the channel.

Spanwise averaged baseline Stanton numbers are compared to empirical relationships, Kays and Crawford [Ref.

13], to verify measurement procedures. The first empirical relationship is for constant wall temperature downstream of an unheated starting length, ε, given by,

$$St_x Pr^{0.4} = 0.0287 Re_x^{-0.2}[1 - (\varepsilon/x)^{9/10}]^{-1/9} \qquad (3.1)$$

This solution is a basic building block for construction of solutions for variable wall temperature solutions.

The next empirical relationship is for a turbulent boundary layer with an unheated starting length followed by a step change to a constant wall heat flux. This relation is given by:

$$St_x Pr^{0.4} = 0.030 Re_x^{-0.2}[1 - (\varepsilon/x)^{9/10}]^{-1/9} \qquad (3.2)$$

The final empirical relationship provides the most exact equation to account for a constant heat flux surface downstream of an unheated starting length. This equation is given by:

$$St_x Pr^{0.4} = 0.030 Re_x^{-0.2}\left[\frac{\beta_1(1/9,10/9)}{\beta_{u_1}(1/9,10/9)}\right] \qquad (3.3)$$

Here, β_1 and β_{u_1} are analytically determined values of the complete Beta function and the incomplete Beta function, respectively.

The three experimental data sets are compared with Equations 3.1, 3.2 and 3.3 in Figure 5. All three baseline Stanton number data sets showed agreement with Equation 3.3 with a maximum deviation of about ±5 percent.

2. Normalized Stanton Number Measurements with an Embedded Vortex

Local Stanton number ratios (St/St_o) with an embedded vortex are shown in Figure 6 for x coordinate locations at 1.15, 1.25, 1.40, 1.60, 1.80 and 2.00 m. Here x is measured from the upstream edge of the trip. The symbol St corresponds to Stanton number values with an embedded vortex and St_o represents the Stanton number baseline values with no embedded vortex. Freestream velocity was held constant at 10.0 ± 0.02 m/s and the test plate heat flux was set with an input of 54.5 ± 0.1 volts and 6.0 amps.

To prevent plotting data points on top of one another and to clarify the streamwise development, the St/St_o axis is expanded between $St/St_o = 0.9$ and $St/St_o = 1.1$ in Figure 6. Areas of high heat transfer are located where Stanton number ratio magnitudes are greater than 1.0 (vortex downwash region) and low heat transfer regions located where Stanton number ratio magnitudes are less than 1.0 (vortex upwash region). The peak value of Stanton number ratio shifts in the positive z-direction as the streamwise distance increases. These results show good

agreement with Ortiz [Ref. 10], Joseph [Ref. 11] and Williams [Ref. 12].

B. VORTEX PAIRS

1. Heat Transfer Measurements

a. Common Downwash

Local St/St_o ratio distributions measured in a boundary layer having an embedded vortex pair with common downwash are present in Figures 7-11. These data are given for different generator spacings b, where b is the distance between the two vortex generator base midpoints described in Section II.B. Freestream velocity is 10.0 ± 0.2 m/s and b values are 2.54, 3.81, 5.08, 6.35 and 7.62 cm. The test plate heat flux was set using 53.3 ± 0.1 volts and 5.9 ± 0.1 amps.

In Figures 7-11, the downwash is located between the vortices in each pair. Consequently, the turbulent boundary layer in the downwash region is diverging with significant lateral strain and St/St_o ratio magnitudes are greater than 1.0. Referring to results in each Figure 7-11, spanwise extents of high heat transfer regions increase with streamwise distance. This is because the vortices and the boundary layer between them are both diverging. Increasing b also results in larger downwash regions in the lateral direction because the initial spanwise spacing of the vortices in each pair is larger. This increased downwash region results in an increased area where St/St_o is greater

than 1.0. This is best seen by comparing Figure 7 and Figure 11. Figure 7 shows St/St_o greater than 1.0 from z = -5.0 cm to z = 5.0 cm for b = 2.54 cm. For Figure 11 results, b = 7.62 cm and St/St_o greater than 1.0 extends from z = -7.0 cm to z = 7.0 cm. Maximum St/St_o in the downwash region also increases as the spacing between the vortices in a pair, increases. In Figure 7, maximum St/St_o is 1.1. In figure 11, maximum St/St_o is 1.2.

b. Common Upwash

St/St_o distributions measured with vortices in pairs having common upwash regions are presented in Figures 12-16. These results are given for different b, which give different spacings between the vortices in each pair. The symbol b is the distance between the vortex generator base midpoints, as described in Section II.B. Freestream velocity is 10.0 ± 0.2 m/s for these results and b = 2.54, 3.81, 5.08, 6.35 and 7.62 cm. 53.6 ± 0.1 volts and 5.9 ± 0.1 amps were used to set the test plate heat flux.

In Figures 12-16, the vortex upwash region is located between the vortices near the wind tunnel center span (z = 0.0 cm). Overall, perturbations to local St/St_o are less than when the downwash is common between the vortices in a pair. Figures 12 and 13 for b = 2.54 cm and b = 3.81 cm show little spanwise variation of St/St_o at different streamwise locations. The slight decrease of St/St_o from the downwash is more apparent in Figures 14-16.

Here, b = 5.08, 6.35 and 7.62 cm, the spanwise regions affected by the upwash range from z = -2.5 cm to z = 2.5 cm. Little changes are evident as the spacing of the vortices in a pair are altered.

2. Secondary Flow Vectors, Streamwise Velocity Distributions, Total Pressure Distributions and Streamwise Vorticity Distributions for Vortex Pair Configurations with Common Downwash

Secondary flow vectors, streamwise velocity, total pressure distributions and streamwise vorticity distributions are presented in Figures 17-28 for vortex pairs with common downwash. Data for b = 2.54 cm are given in Figures 17-20, data for b = 5.08 cm are given in Figures 21-24, and data for b = 7.62 cm are given in Figures 25-28. For these data, freestream velocity is 10.0 ± 0.2 m/s and test plate heat flux was set using 53.3 ± 0.1 volts and 5.9 ± 0.1 amps.

Vortices are indicated in Figures 17, 21 and 25 by clockwise and counterclockwise rotating secondary flow vectors. It is evident that the downwash exists between the vortices in each pair, such that the vortex on the left is clockwise rotating and the vortex on the right is counter-clockwise rotating. Other significant secondary flows are evidence everywhere near the vortex, particularly beneath the vortex centers near the wall. In these views, freestream flow direction is into the page.

Distributions of streamwise velocity and total pressure in Figures 18, 19, 22, 23, 26 and 27 show that the

local boundary layer thickness is increased in the upwash region. This is because low momentum fluid is convected away from the wall into the upwash by the secondary flows. The combination of low streamwise velocities near the wall and increased boundary layer thickness account for St/St_o values less than 1.0 shown in Figures 7-11.

In the downwash region, high velocity freestream fluid is brought close to the wall by the secondary flows. Consequently, the local boundary layer is very thin. Corresponding St/St_o values are greater than 1.0 in Figures 7-11.

Figures 18, 19, 22, 23, 26 and 27 also show streamwise velocity and total pressure deficits near the centers of vortices. These are caused by the wake from the vortex generators, which is rolled into the vortex core by the secondary flows.

Figures 20, 24 and 28 show vorticity contours. The vortex center is the location of maximum vorticity. For b = 2.54 cm, vortex centers are located at z = -5.0 cm and z = 6.0 cm. For b = 5.08 cm, vortex centers are located at z = -7.0 cm and z = 6.5 cm.

C. VORTEX ARRAYS

1. Heat Transfer Measurements

St/St_o distributions measured beneath vortex arrays are presented in Figures 29-32. The details of the vortex array dimensions are discussed in Section II.B. Figures 29,

30 and 31 correspond to b = 3.81, 5.08 and 6.35 cm with the vortex generators arranged such that downwash exists at z = 0.0 cm. Figure 32 gives data for b = 6.35 cm where vortex generators are arranged such that upwash exists at z = 0.0 cm. b is defined as shown on Figure 4. For these four cases, freestream velocity is 10.0 ± 0.2 m/s and test plate heat flux was set using 54.5 ± 0.1 volts and 6.0 ± 0.1 amps.

In Figures 29-32, St/St_o values are generally greater than 1.0 beneath downwash regions and less than 1.0 beneath upwash regions. As b decreases, spanwise extents of downwash regions increase. Figure 29 shows St/St_o greater than 1.0 at x = 2.00 m from z = -2.5 cm to z = 2.5 cm. Here, b = 3.81 cm. Figure 31 shows data for b = 6.35 cm. Regions where St/St_o is greater than 1.0 extend from z = -4.5 cm to z = 4.5 cm at x = 2.00 m. In Figure 32, St/St_o is less than 1.0 for z = -2.0 cm to z = 2.0 cm.

2. Secondary Flow Vectors, Streamwise Velocity Distributions, Total Pressure Distributions and Streamwise Vorticity Distributions for Common Downwash Configurations

Two sets of secondary flow vectors, streamwise velocity distributions, total pressure distributions and streamwise vorticity distributions are presented in Figures 33-40. These data were obtained using b = 5.08 cm and b = 6.35 cm with generators arranged such that vortex downwash regions exist near z = 0.0 cm.

Extents and locations of vortices are indicated by secondary flow vectors in Figures 33 and 37. The

characteristics of these vortices are similar to the characteristics of the vortices in pairs with several exceptions. First, vortices in paired configurations diverge and converge with streamwise development. In contrast, the vortices in the arrays tend to move in the streamwise direction without significant convergence and divergence. In both cases, the vortices with common upwash between them tend to move closer together with streamwise development because of the differences in pressure between each side of each vortex. Also particularly noticeable, especially for the arrays, are compacated and intensified upwash regions which tend to cause adjacent vortices to move away from the wall. Such motion is also a result of the pressure distribution which results as fluid is rearranged by secondary flows.

Streamwise velocity contours are given in Figures 34 and 38. The proximity of vortex pairs with common upwash is responsible for mushroom-shaped contours. The stem of this mushroom-shape is the location of low momentum fluid which is convected away from the wall by the upwash region. The corresponding wall region is one of low St/St_o. In the downwash region, high velocity freestream fluid is near the wall because of downwash secondary flows. Here, the boundary layer is thin and St/St_o are greater than 1.0. Total pressure contours in Figures 35 and 39 show similar characteristics.

Corresponding vorticity contours are given in Figures 36 and 40. For the b = 5.08 cm data, vortex centers are located at z = -4.0 cm and z = 4.0 cm. For b = 6.35 cm data, vortex centers are located at z = -3.0 cm and z = 6.0 cm.

IV. COMPARISON TO VORTEX ARRAYS DEVELOPING FROM CENTRIFUGAL INSTABILITIES IN A CURVED CHANNEL

Figures 41-48 present streamwise velocity and total pressure distributions measured in a 40:1 aspect ratio channel with mild curvature. These measurements were made 19.0 cm downstream of the end of curvature. Methods developed by Baun [Ref. 14] were used to collect these data for Dean numbers from 50 to 150. Samples of Baun's [Ref. 14] data measured 120° from the start of curvature are shown in Figures 49 and 50. These data are compared with streamwise velocity and total pressure distributions shown in Figures 34, 35, 38 and 39, which were measured in artificially induced vortices. Data are time-averaged in all of these figures.

Baun's [Ref. 14] streamwise velocity and total pressure contours (from laminar flow) in Figures 49 and 50 show some similarities with the streamwise velocity and total pressure contours (from artificially induced vortices in turbulent flow) shown in Figures 34, 35, 38 and 39. In both cases, low velocity, low pressure fluid is present in the upwash. For the channel results, this upwash emanates from the concave surface. For both situations, downwash regions correspond to regions of high velocity and high pressure. Downwash regions result in diverging boundary layers and the

upwash regions result in converging boundary layers. The principal reason for flow structure differences in the channel and the boundary layer is that the curved channel was bounded and the straight channel is not constrained on the freestream flow. Thus, vortices in the channel may not move away from the concave surface and expand as they do with respect to the wall of the wind tunnel with freestream. In addition, the continual application of centrifugal instabilities causes curved bounded channel vortices to become stronger as they develop.

Measurements in the heat transfer curved channel 19.0 cm downstream of the end of curvature produced velocity and pressure contours which do not show distinct evidence of vortices. Instead, flow is approximately spanwise uniform for Dean numbers from 50 to 150, as shown by the data in Figures 41-48. These results are different from Baun's [Ref. 14], because streamwise locations are further downstream. Because of this, the flow is believed to be more unsteady, especially in the spanwise direction, and consequently, time-averaged results show spanwise uniform characteristics.

V. SUMMARY AND CONCLUSIONS

Vortex pairs and vortex arrays were studied which: (1) were induced artificially using half delta wings on the floor of a wind tunnel, and (2) developed naturally as a result of centrifugal instabilities in a curved rectangular channel with a 40:1 aspect ratio.

Measurements in the artificially induced vortex pairs show regions of common downwash, where streamwise velocity and total pressures are high. Here, local boundary layer thickness is reduced and heat transfer is augmented compared to two-dimensional flows over flat plates. As flow continues downstream, vortices boardering this common downwash region move further apart resulting in a diverging boundary layer. As the spacing between the vortices in a pair increases, downwash areas span larger distances giving larger regions of high heat transfer.

Regions of low streamwise velocity and low total pressure exist in common upwash regions. Local boundary layer thickness is increased and heat transfer is low compared to two-dimensional flows over flat plates. Vortices bordering the upwash region move closer together as flow develops downstream resulting in a converging boundary layer. Such streamwise vortex motion results because of pressure differences on the sides of the vortices.

The characteristics of the vortices in the arrays are similar to the characteristics of vortices in pairs with several exceptions. First, vortices in paired configurations diverge and converge with streamwise development. In contrast, the vortices in the arrays tend to move in the streamwise direction without significant convergence and divergence. In both cases, the vortices with common upwash between them tend to move closer together with streamwise development because of the differences in pressure between each side of each vortex. Also particularly noticeable, especially for the arrays, are compacted and intensified upwash regions which tend to cause adjacent vortices to move away from the wall.

Measurements in artificially induced vortices show significant similarities to vortices induced by centrifugal instabilities in a curved channel (Baun [Ref. 14]). The artificially induced vortices were generated in an open-circuit, sub-sonic wind tunnel where freestream flow was turbulent with Reynolds numbers of 8.0×10^6 to 1.4×10^6. The vortices induced by centrifugal instabilities were generated in curved channel with laminar flow over a range of Dean numbers of 50 to 150. The most important differences result because one flow is bounded by a wall and one is bounded by a freestream.

APPENDIX A

FIGURES

The following pages contain the figures used in the development of this thesis.

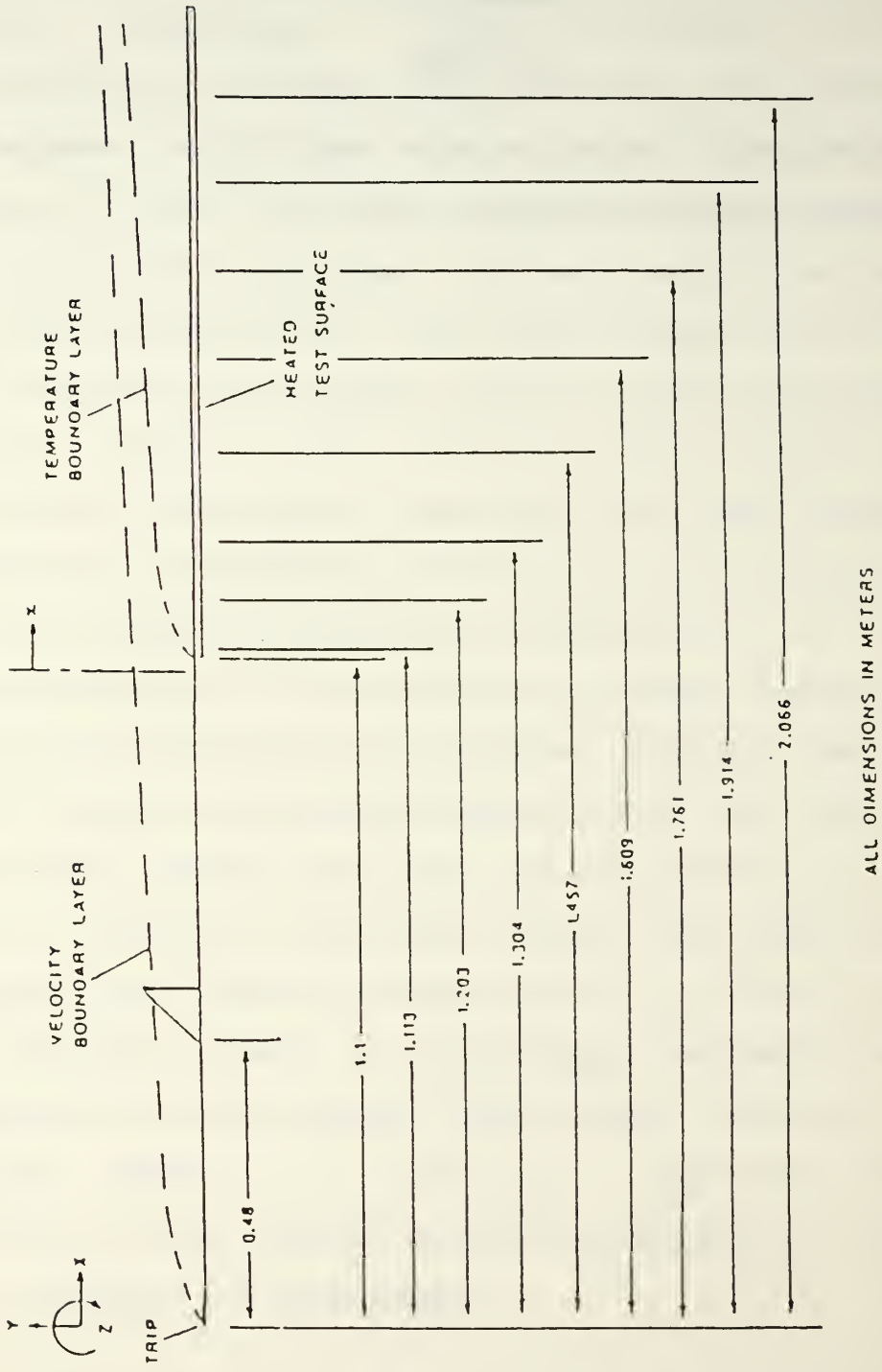

Figure 1. Test Section Coordinate System

VORTEX GENERATOR

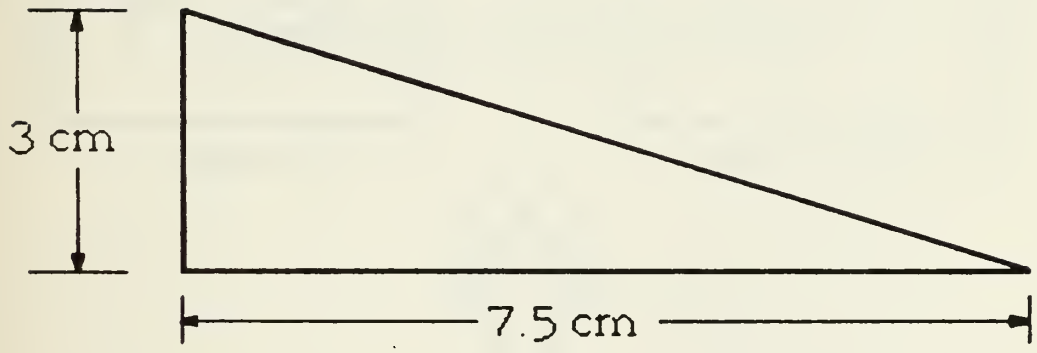

Figure 2. Vortex Generator

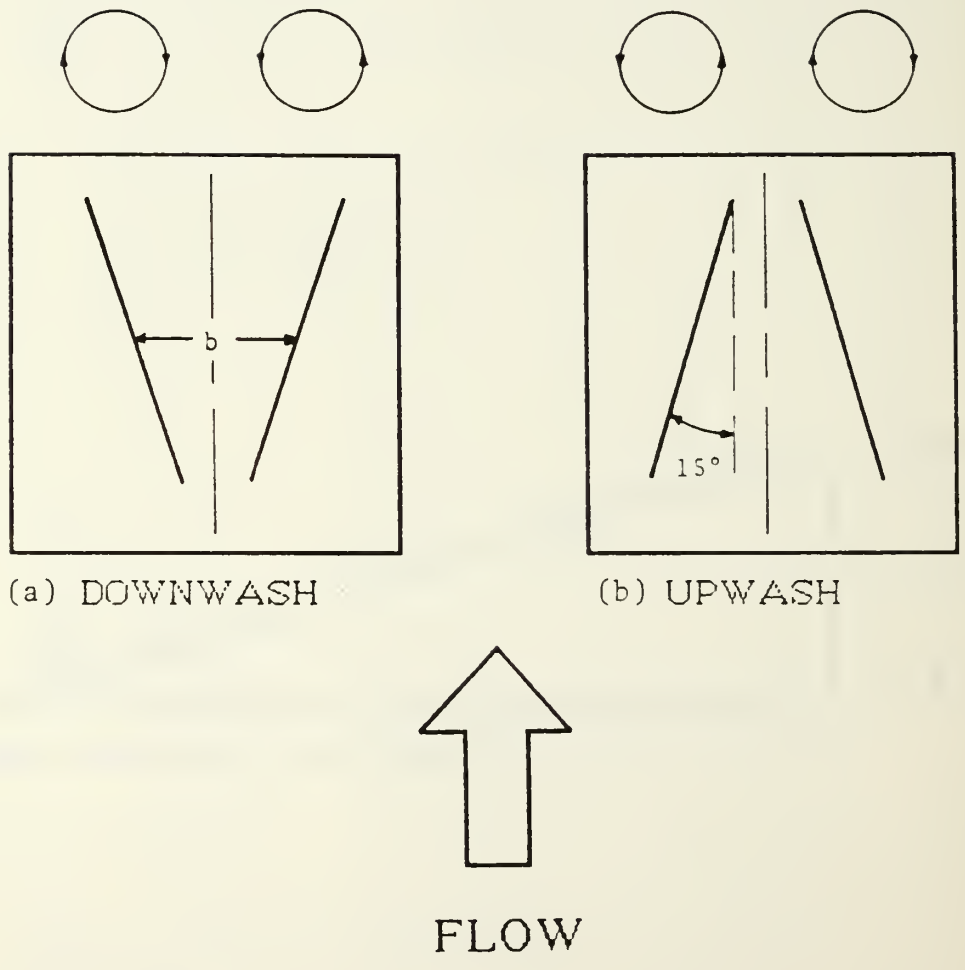

Figure 3. (a) Vortex Pair in Downwash Configuration
(b) Vortex Pair in Upwash Configuration

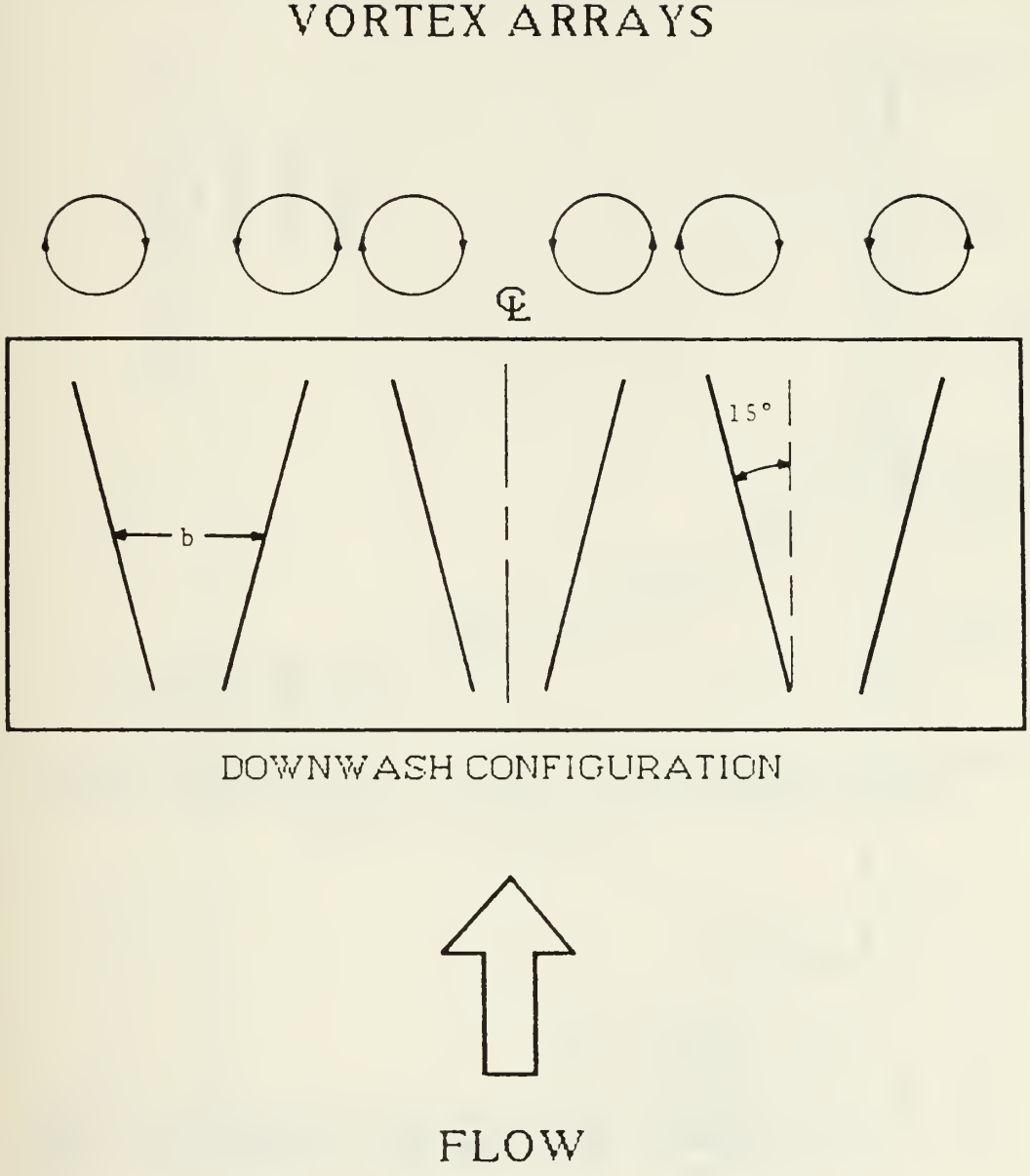

Figure 4. Vortex Array in Downwash Configuration

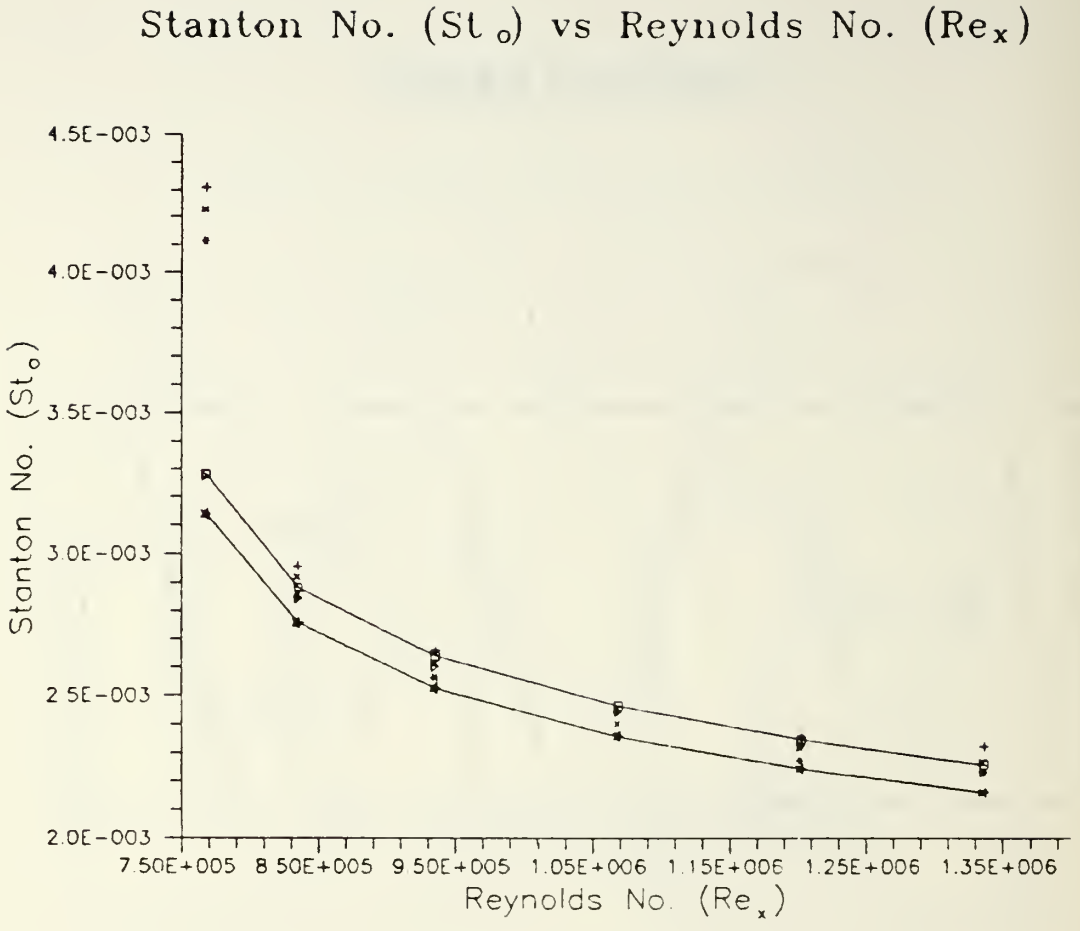

Figure 5. Stanton Number Comparison Between Experimental Measurements and Empirical Relationships

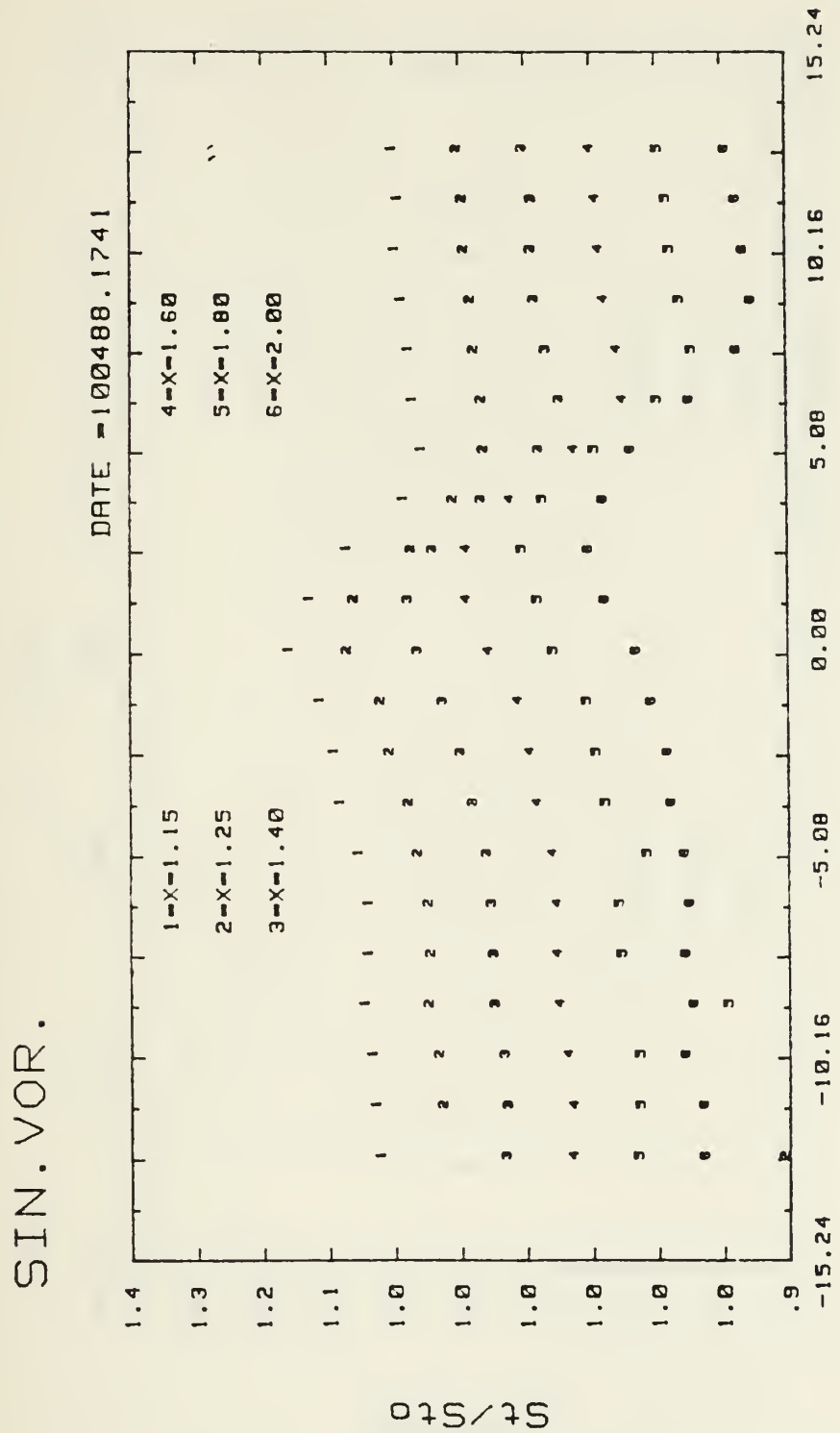

Figure 6. Local St/St_o Ratio Distribution with an Embedded Vortex

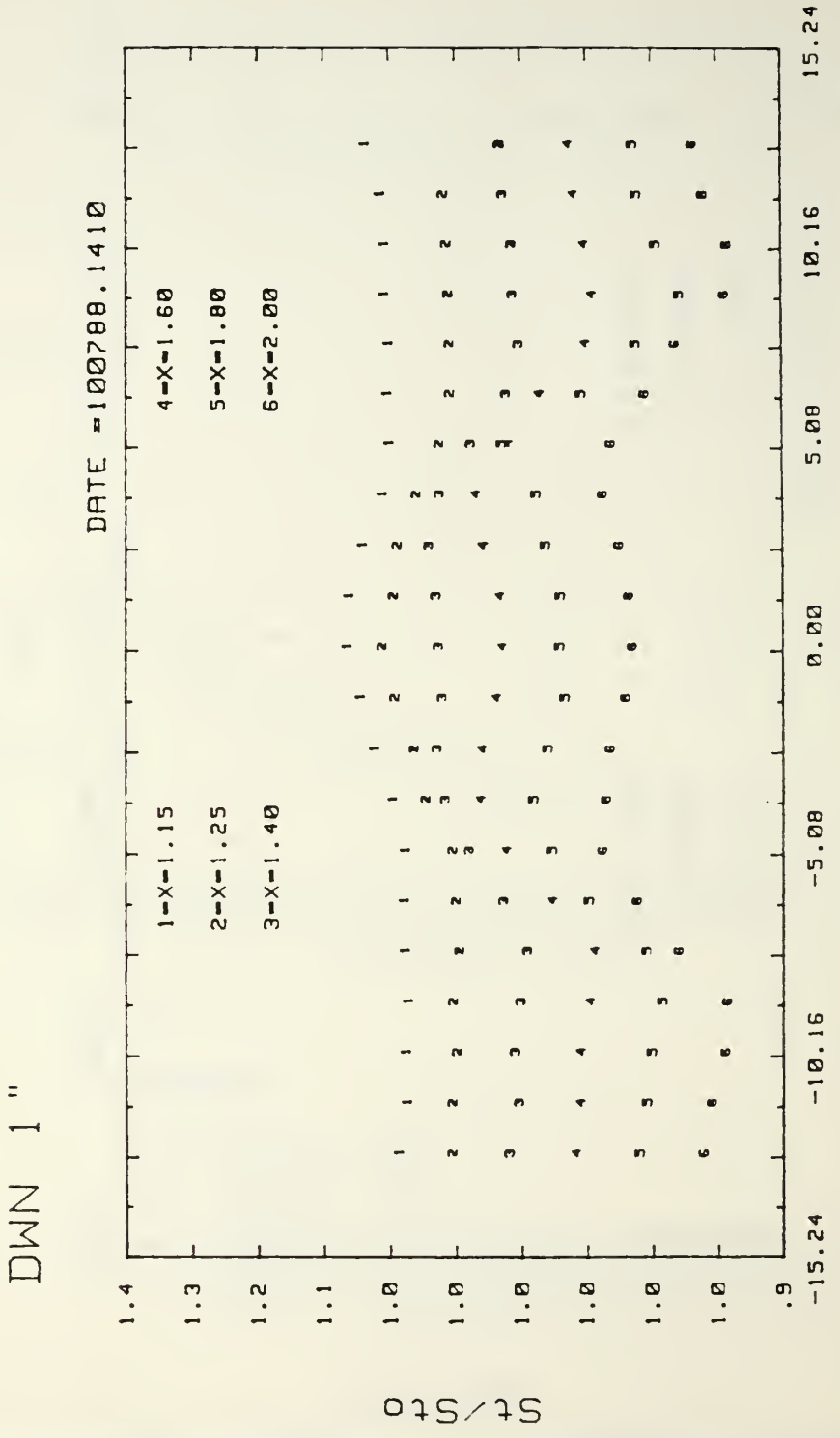

Figure 7. Local St/St_o Ratio Distribution with a Vortex Pair in Downwash Configuration and b = 2.54 cm

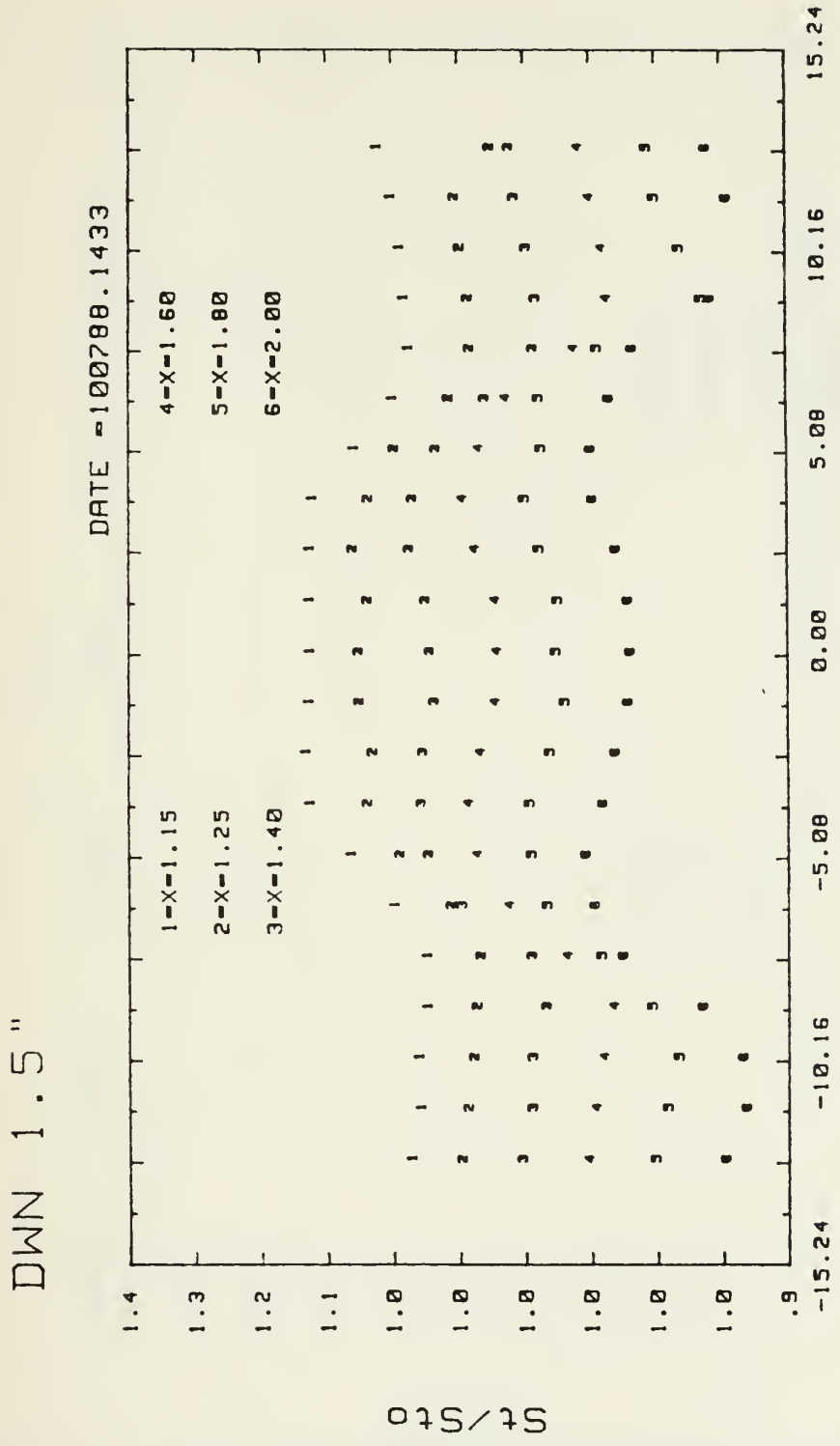

Figure 8. Local St/St_o Ratio Distribution with a Vortex Pair in Downwash Configuration and b = 3.81 cm

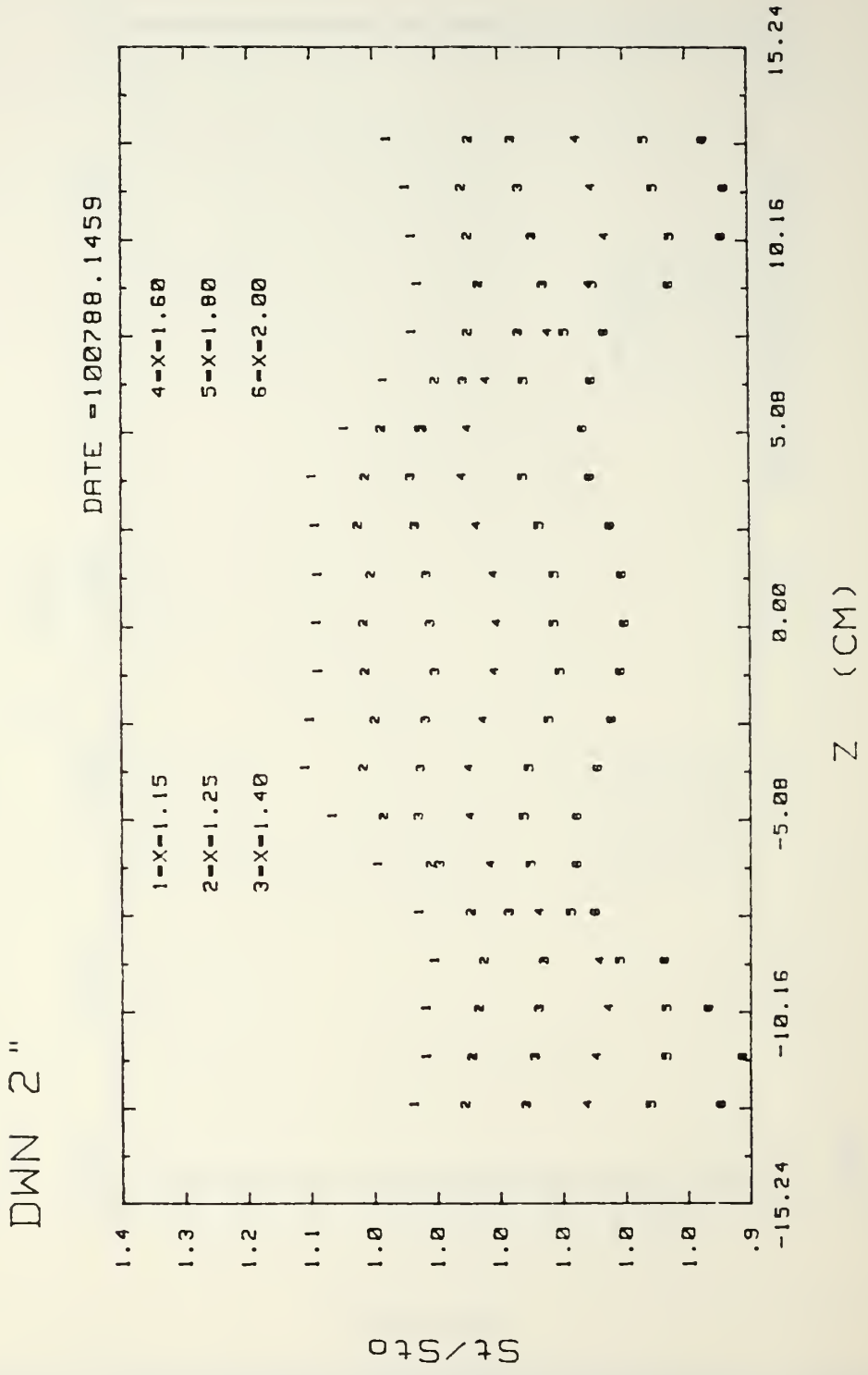

Figure 9. Local St/St_o Ratio Distribution with a Vortex Pair in Downwash Configuration and b = 5.08 cm

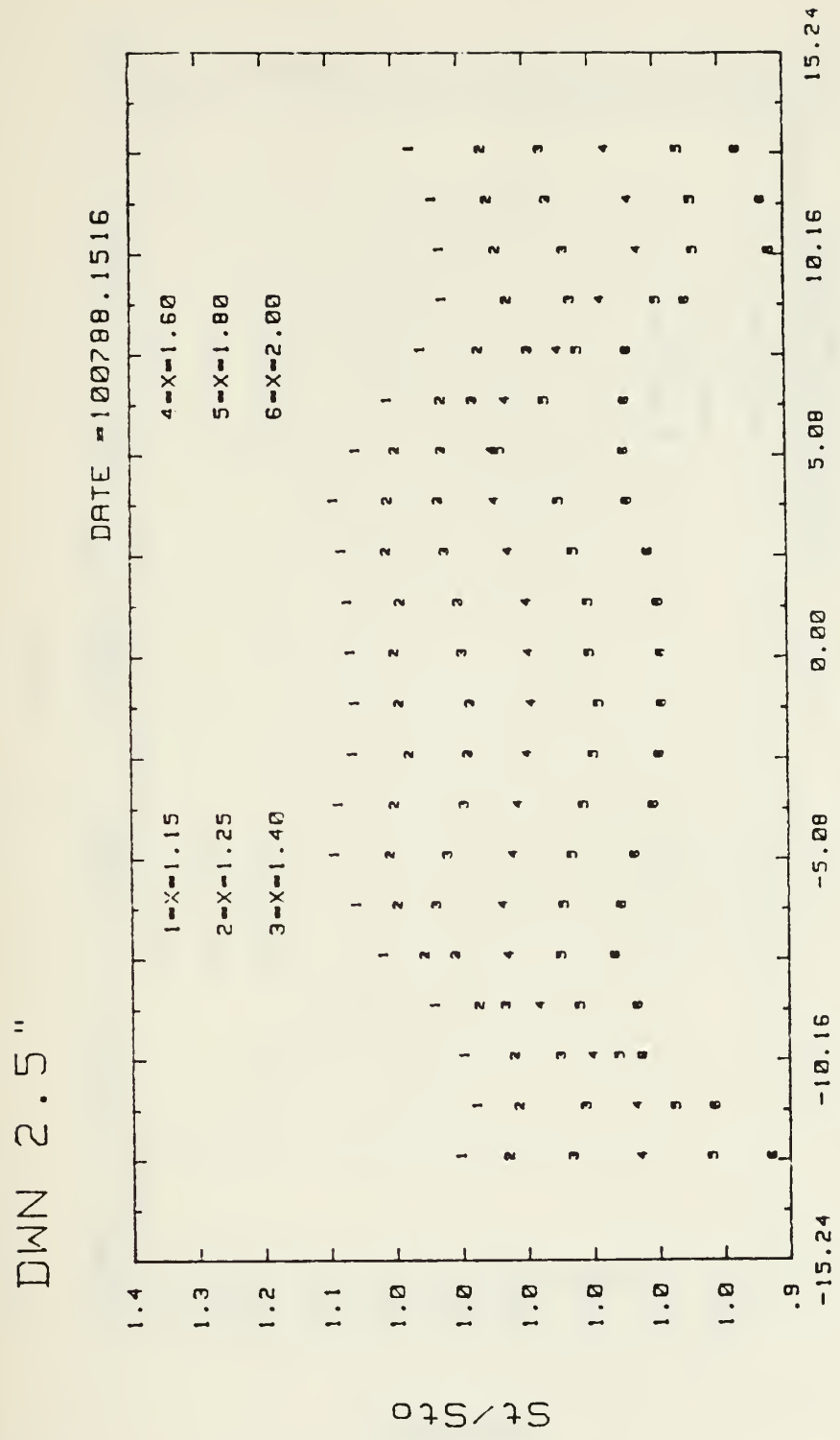

Figure 10. Local St/St_o Ratio Distribution with a Vortex Pair in Downwash Configuration and b = 6.35 cm

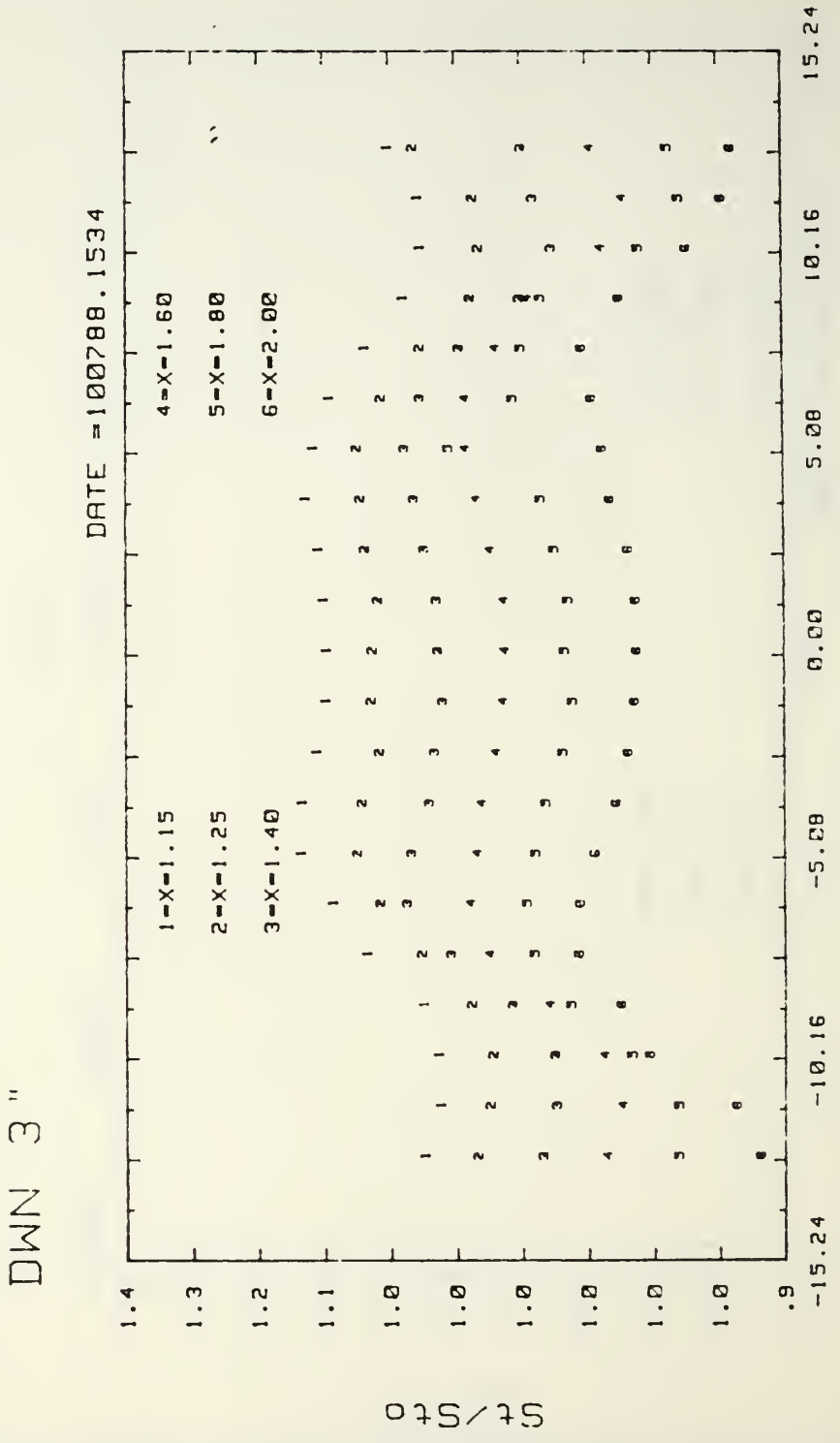

Figure 11. Local St/St_o Ratio Distribution with a Vortex Pair in Downwash Configuration and b = 7.62 cm

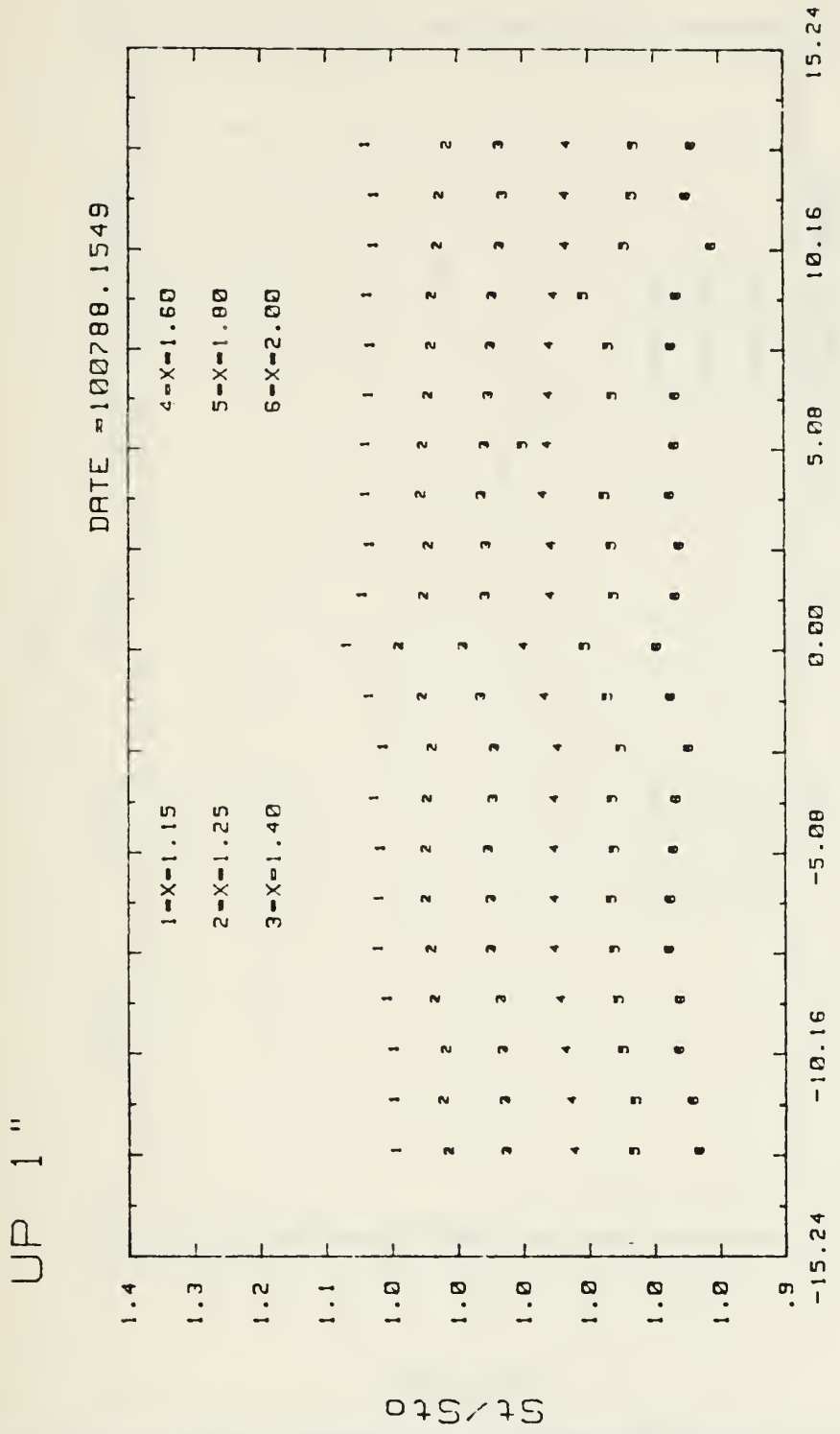

Figure 12. Local St/St_o Ratio Distribution with a Vortex Pair in Upwash Configuration and b = 2.54 cm

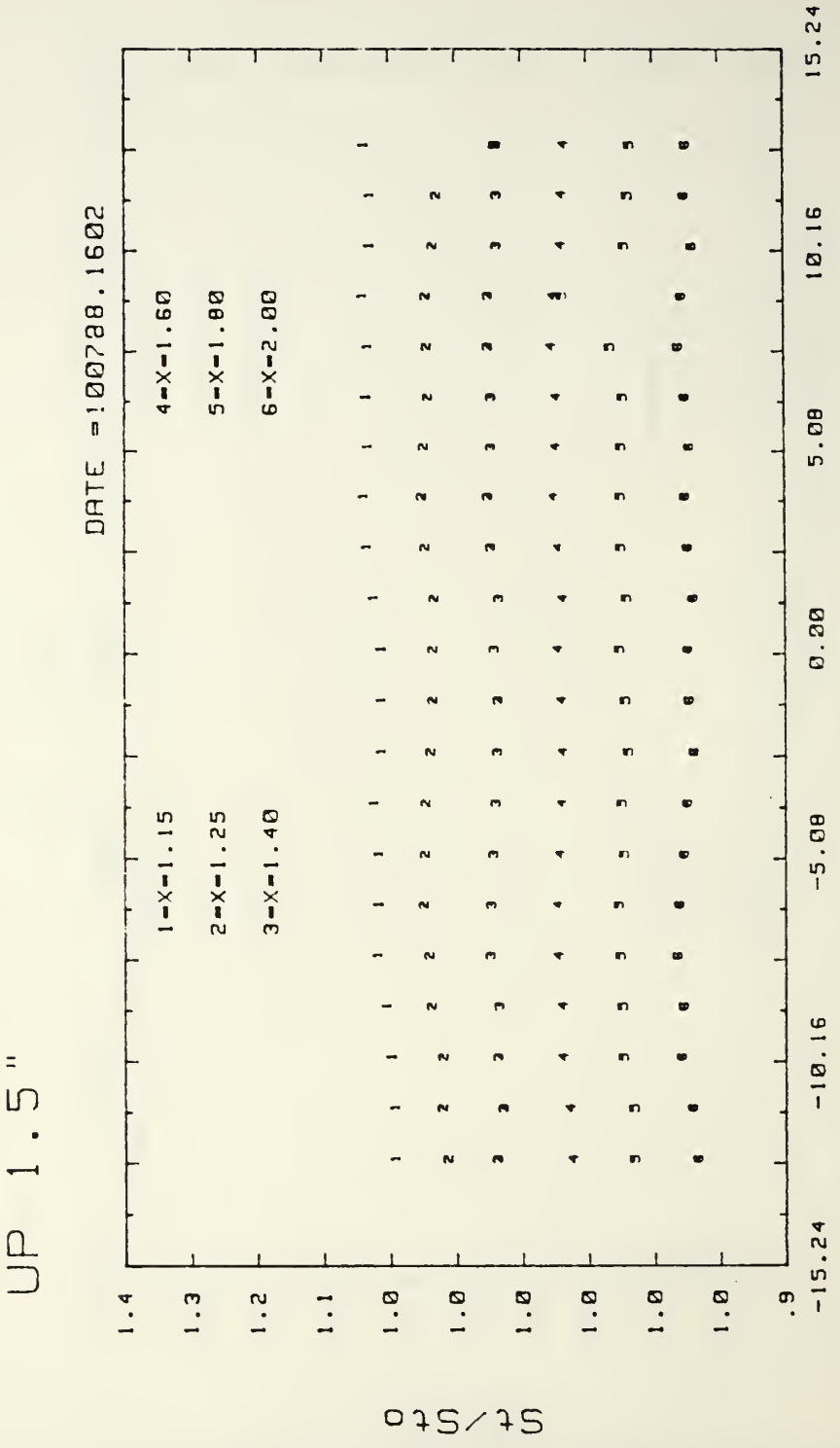

Figure 13. Local St/St_o Ratio Distribution with a Vortex Pair in Upwash Configuration and b = 3.81 cm

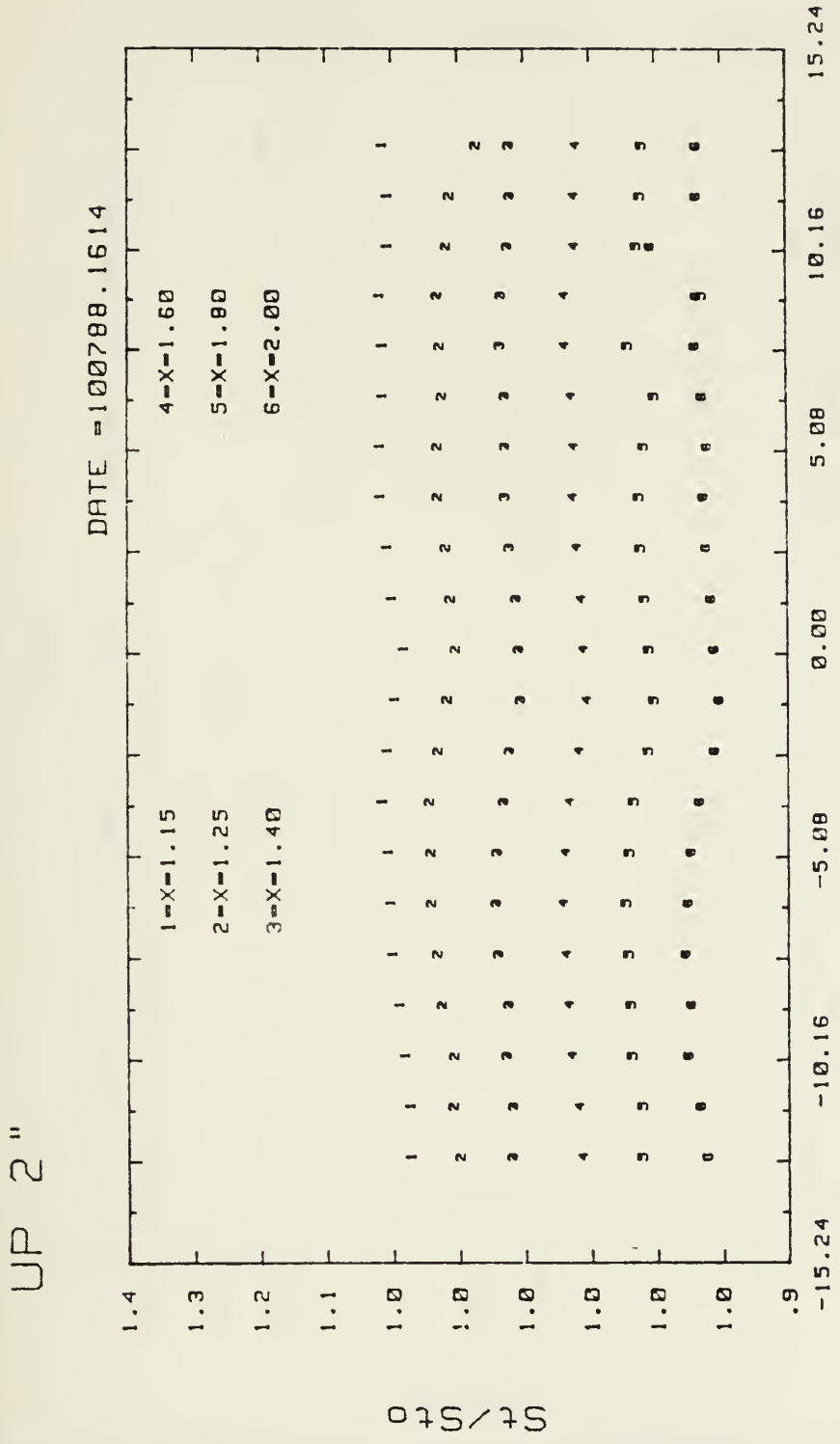

Figure 14. Local St/St_o Ratio Distribution with a Vortex Pair in Upwash Configuration and b = 5.08 cm

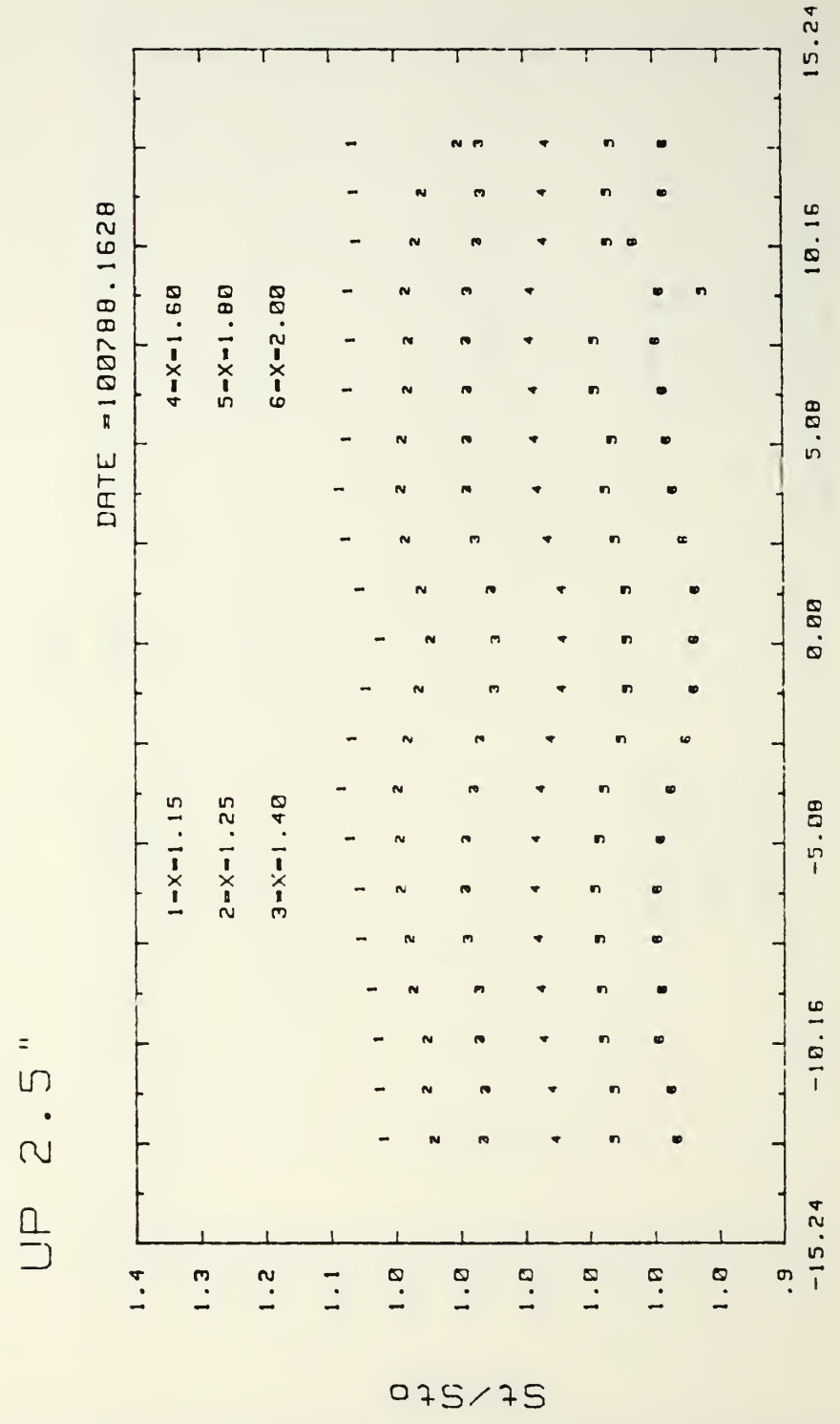

Figure 15. Local St/St_o Ratio Distribution with a Vortex Pair in Upwash Configuration and b = 6.35 cm

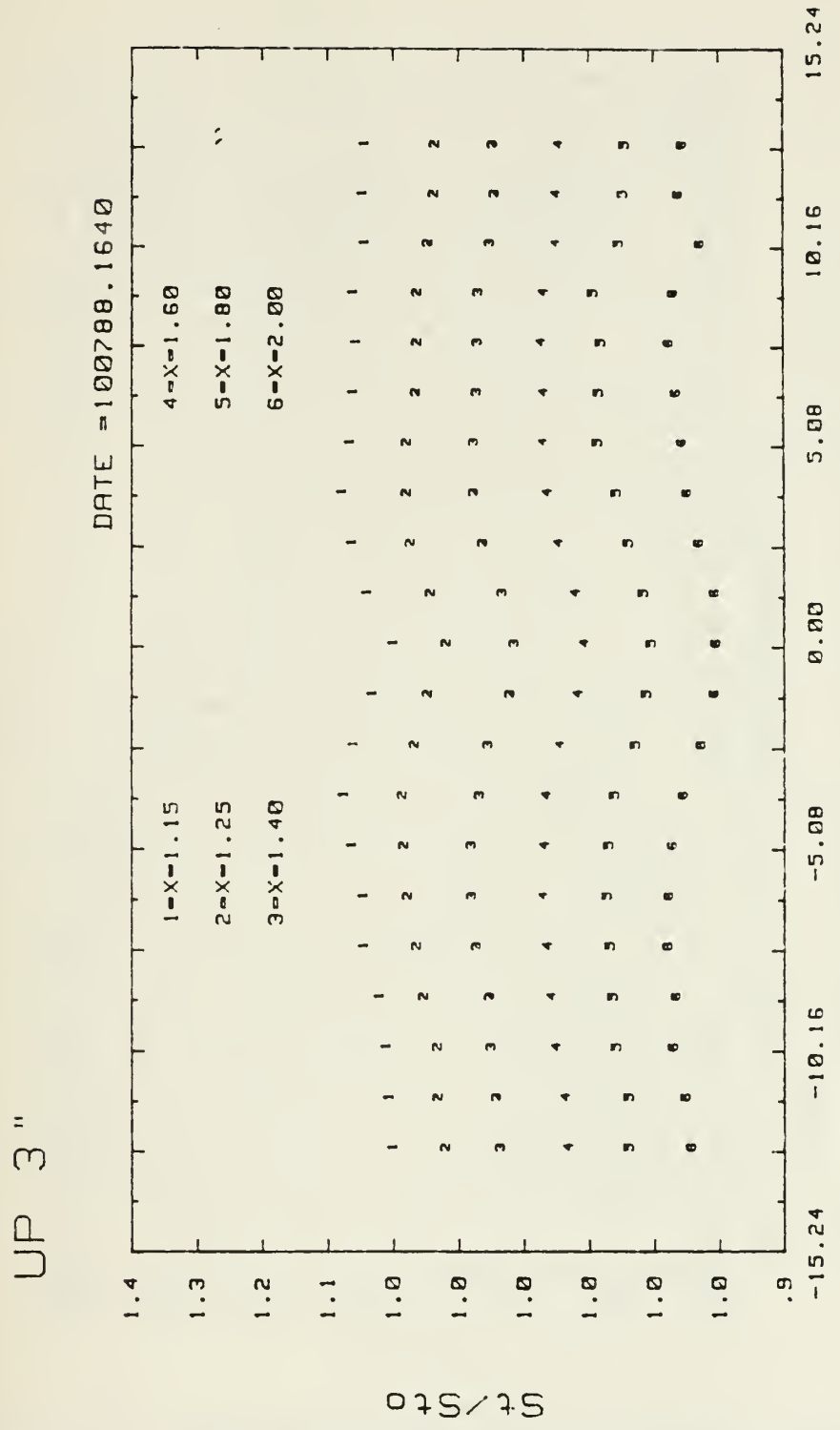

Figure 16. Local St/St_o Ratio Distribution with a Vortex Pair in Upwash Configuration and b = 7.62 cm

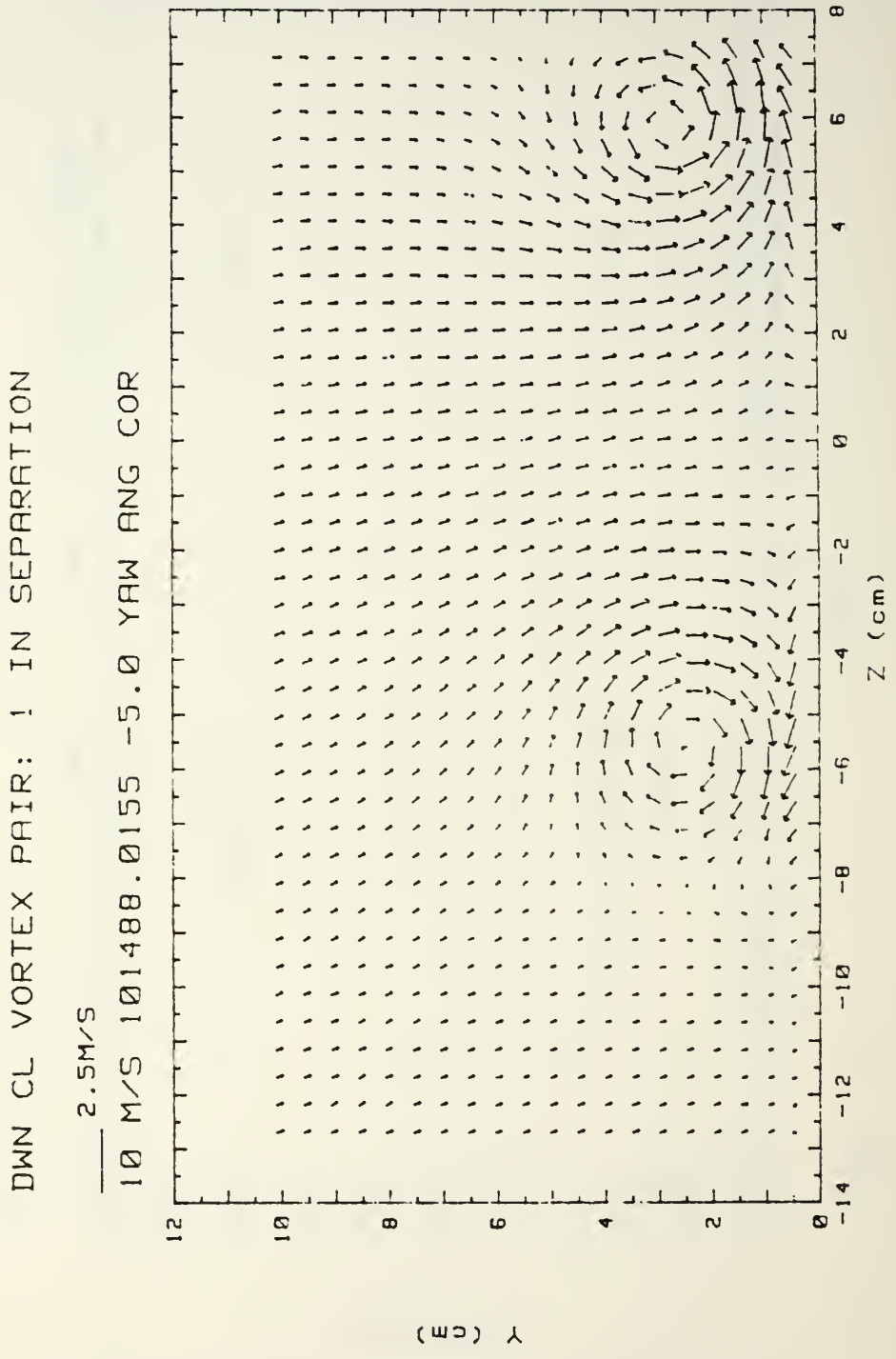

Figure 17. Secondary Flow Vectors in a Boundary Layer with an Embedded Vortex Pair. b = 2.54 cm, U_∞ = 10 m/s

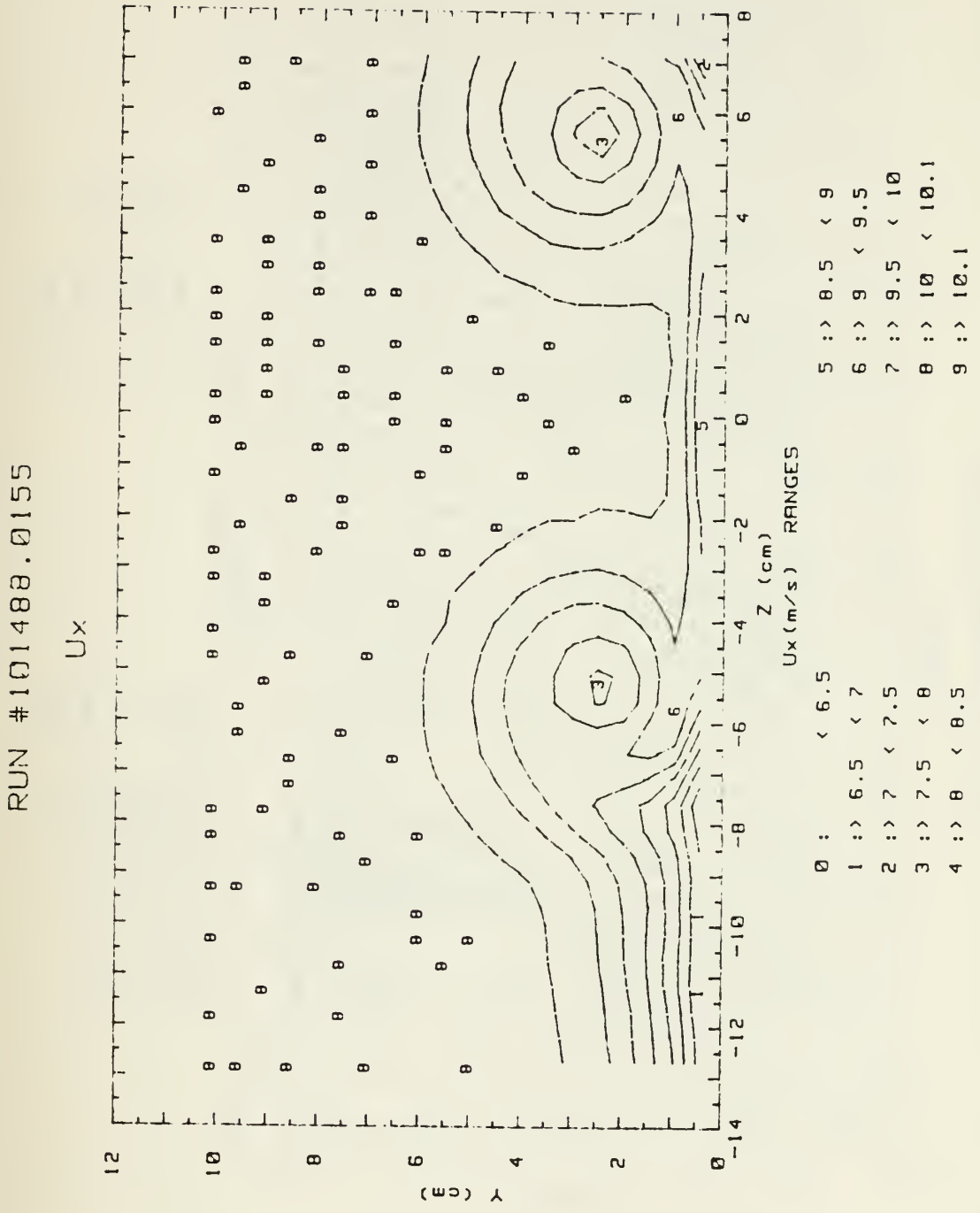

Figure 18. Streamwise Velocity Contours in a Boundary Layer with an Embedded Vortex Pair. b = 2.54 cm, U_∞ = 10 m/s

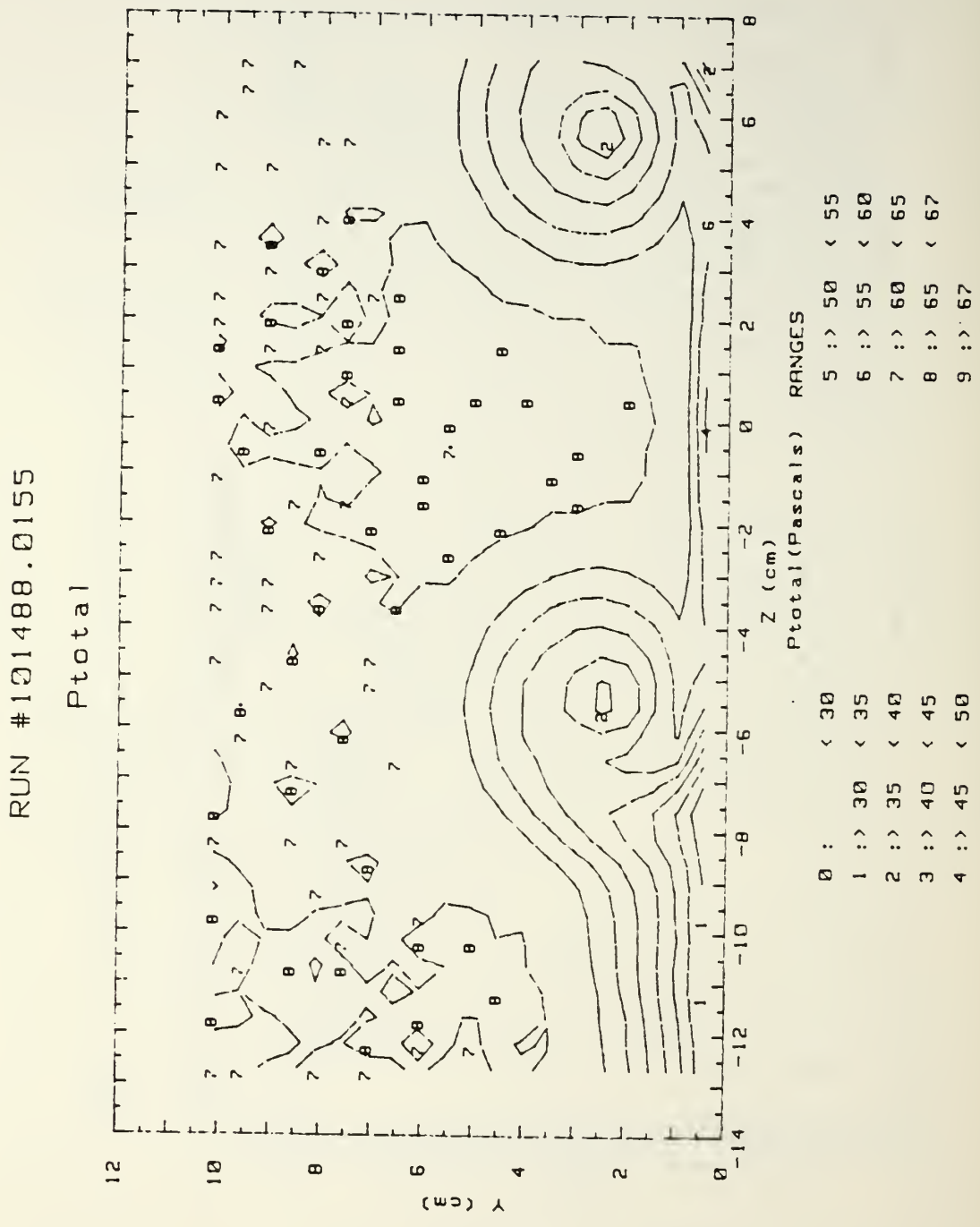

Figure 19. Total Pressure Contours in a Boundary Layer with an Embedded Vortex Pair. b = 2.54 cm, U_∞ = 10 m/s

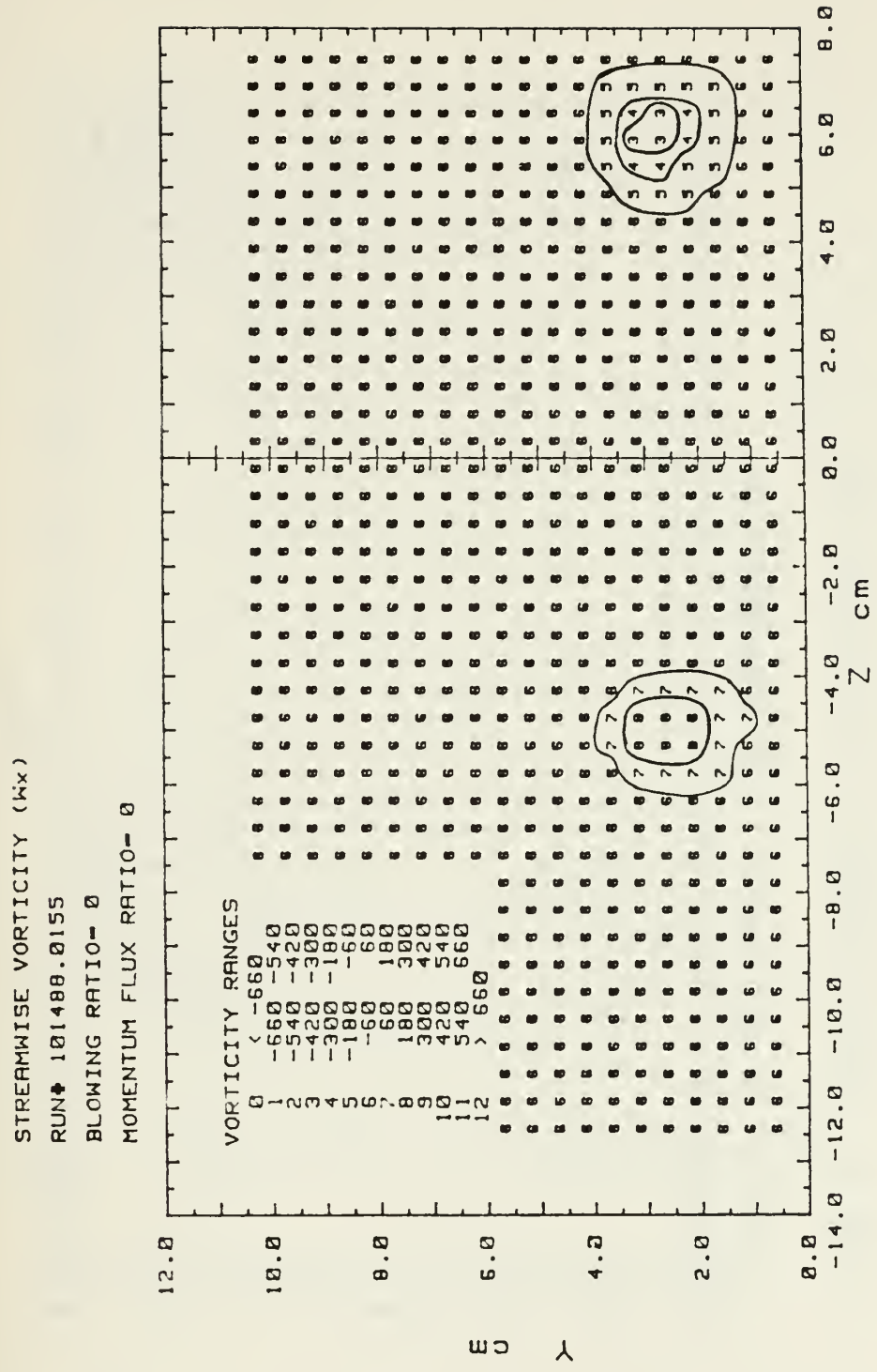

Figure 20. Streamwise Vorticity Contours in a Boundary Layer with an Embedded Vortex Pair. b = 2.54 cm, U_∞ = 10 m/s

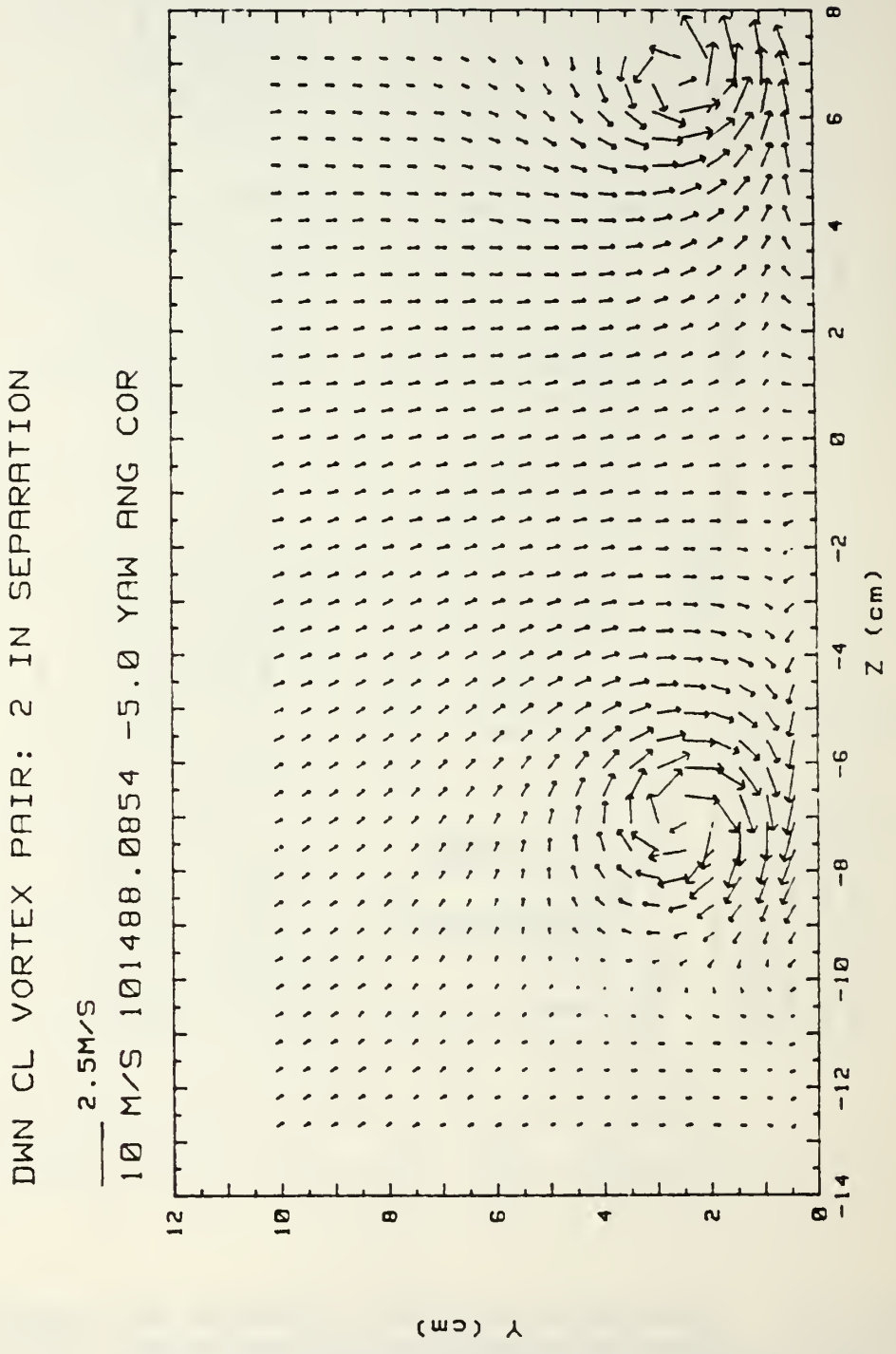

Figure 21. Secondary Flow Vectors in a Boundary Layer with an Embedded Vortex Pair. b = 5.08 cm, U_∞ = 10 m/s

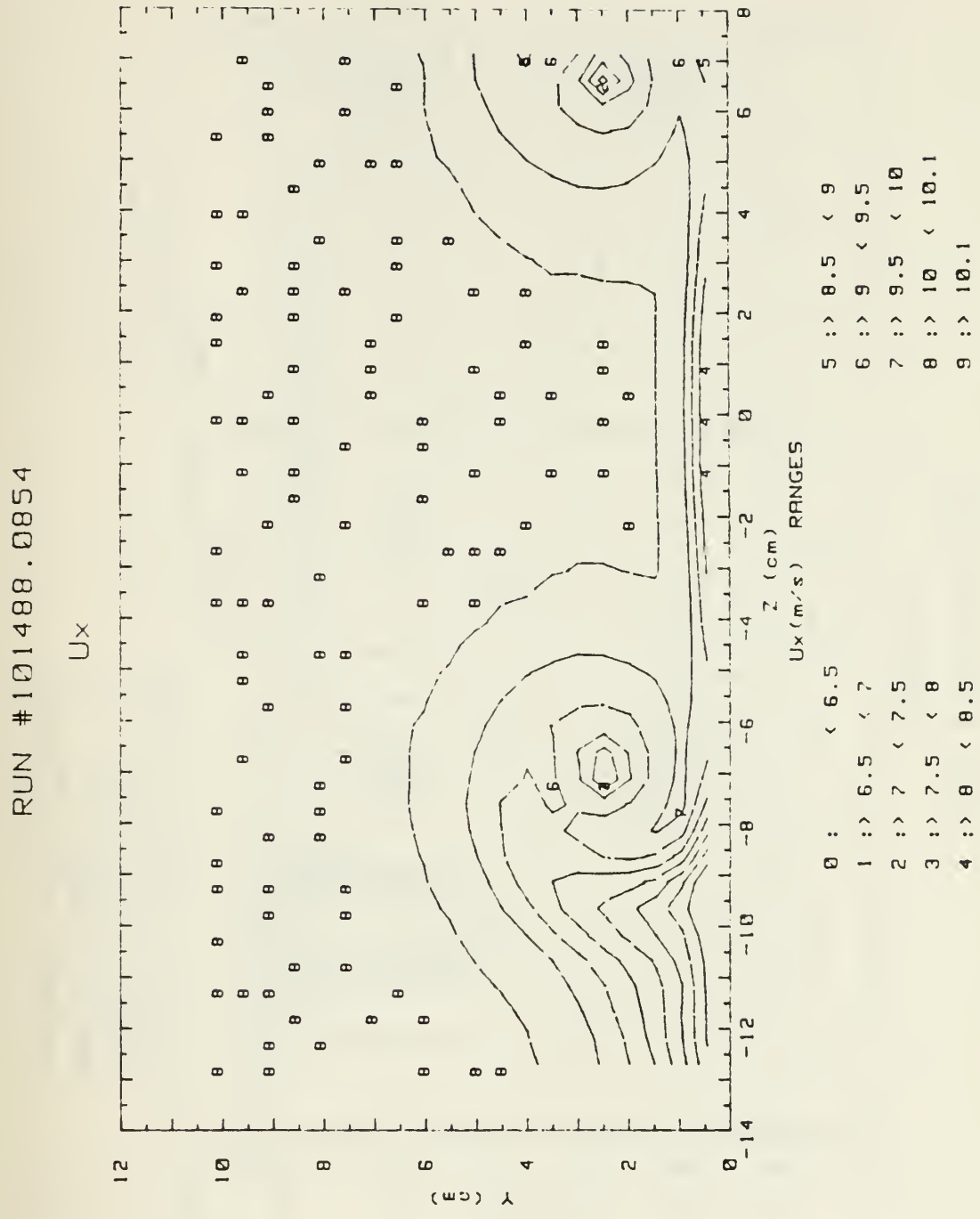

Figure 22. Streamwise Velocity Contours in a Boundary Layer with an Embedded Vortex Pair. b = 5.08 cm, U_∞ = 10 m/s

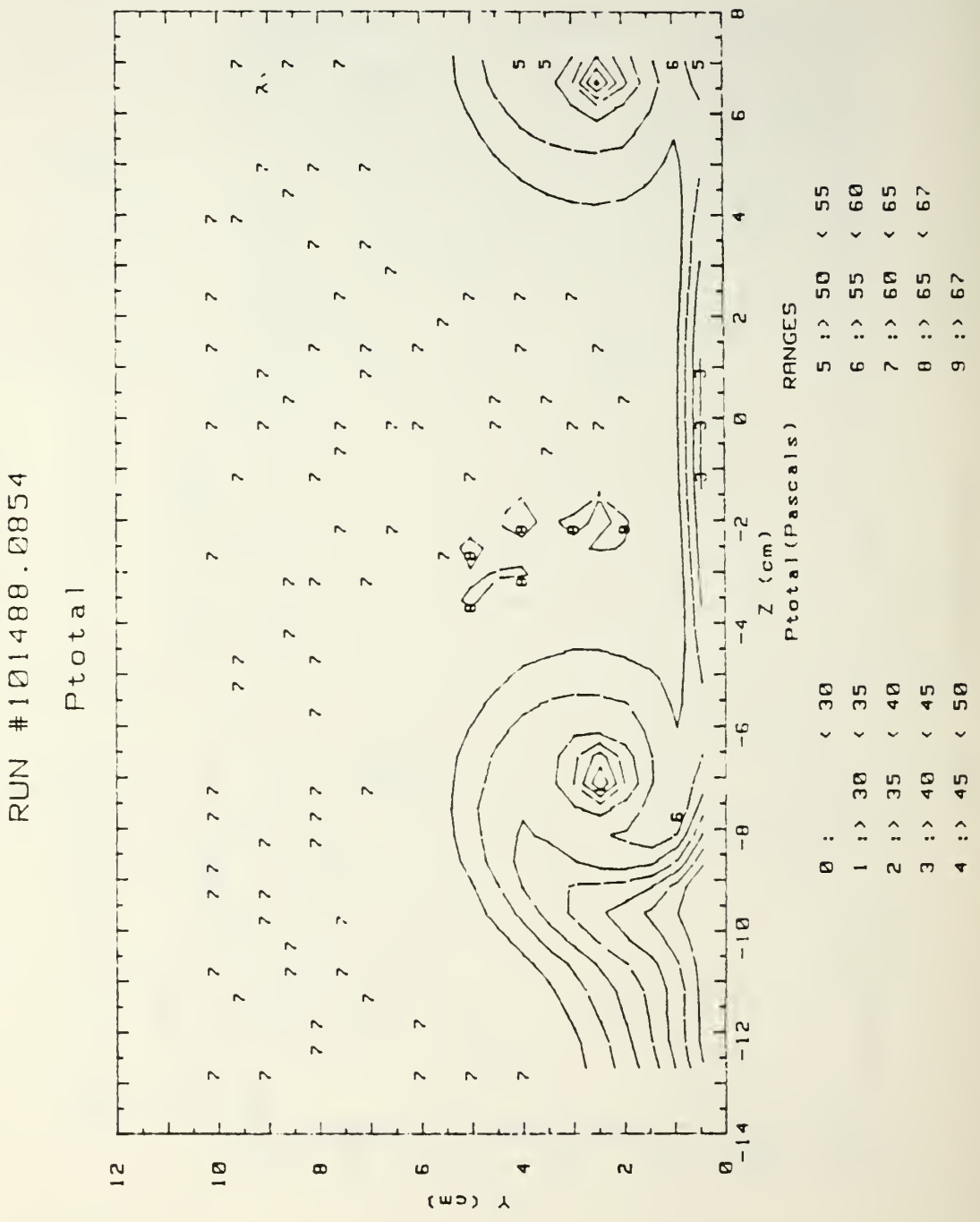

Figure 23. Total Pressure Contours in a Boundary Layer with an Embedded Vortex Pair. b = 5.08 cm, U_∞ = 10 m/s

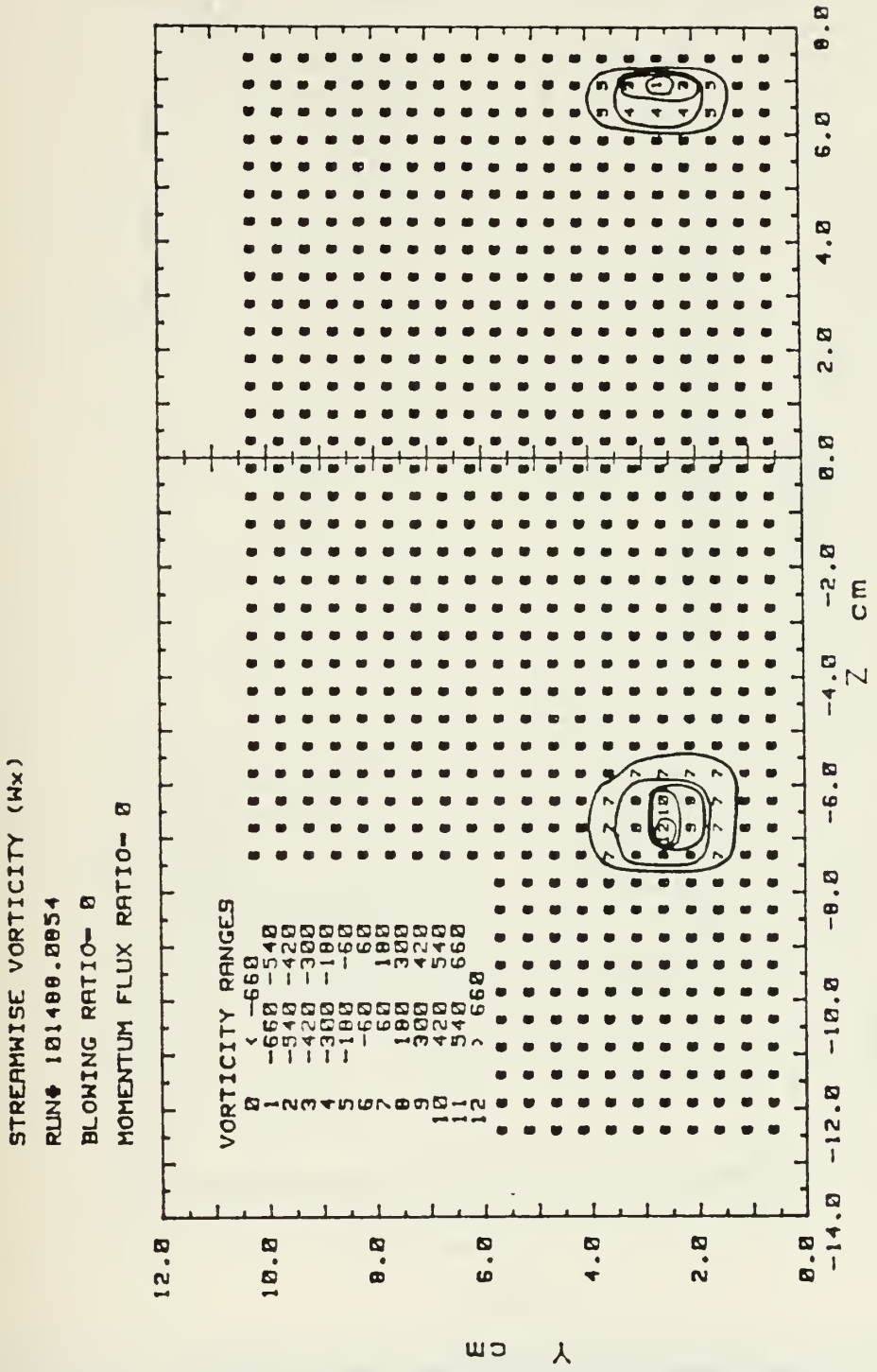

Figure 24. Streamwise Vorticity Contours in a Boundary Layer with an Embedded Vortex Pair.
b = 5.08 cm, U_∞ = 10 m/s

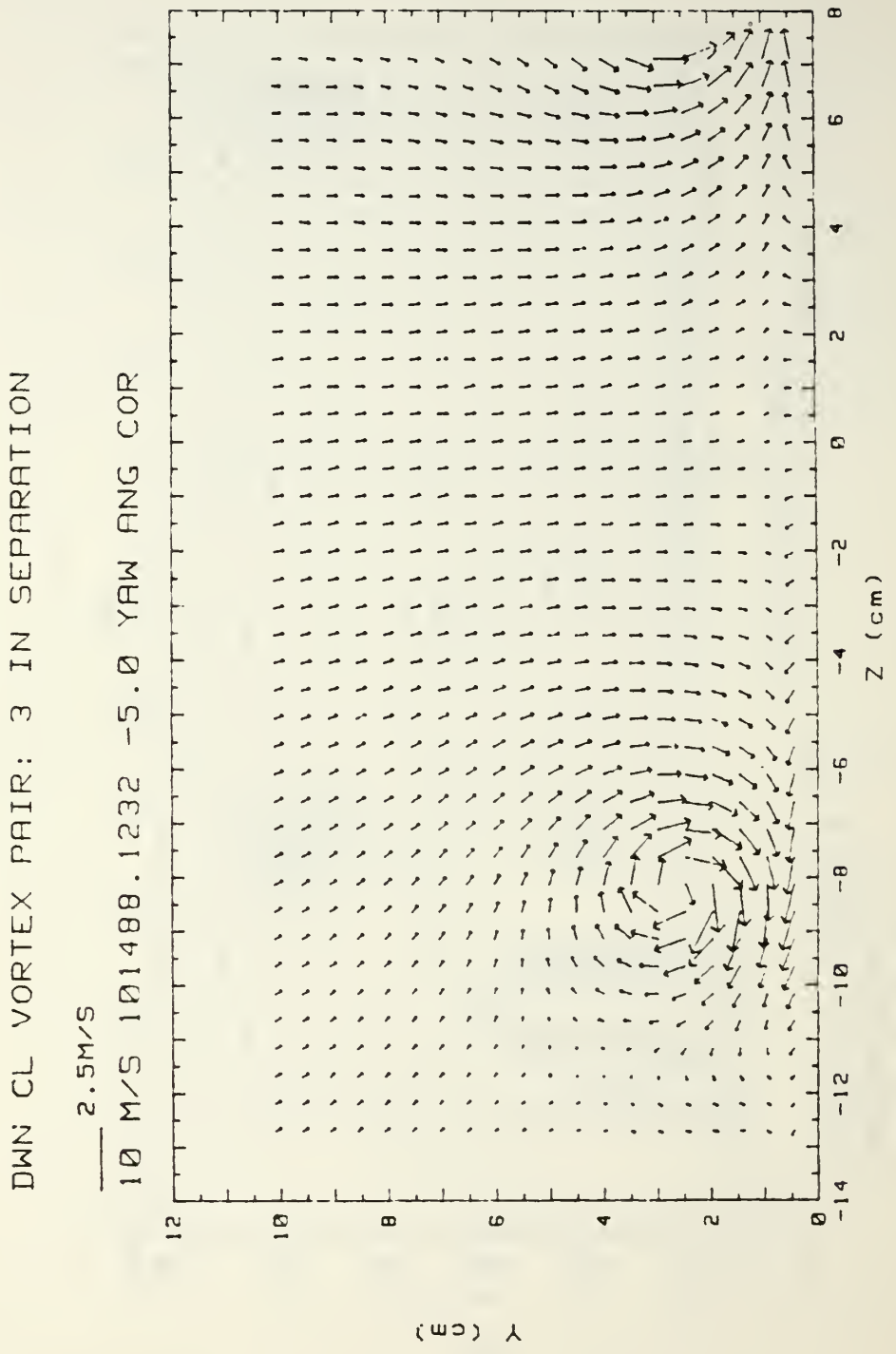

Figure 25. Secondary Flow Vectors in a Boundary Layer with an Embedded Vortex Pair. b = 7.62 cm, U_∞ = 10 m/s

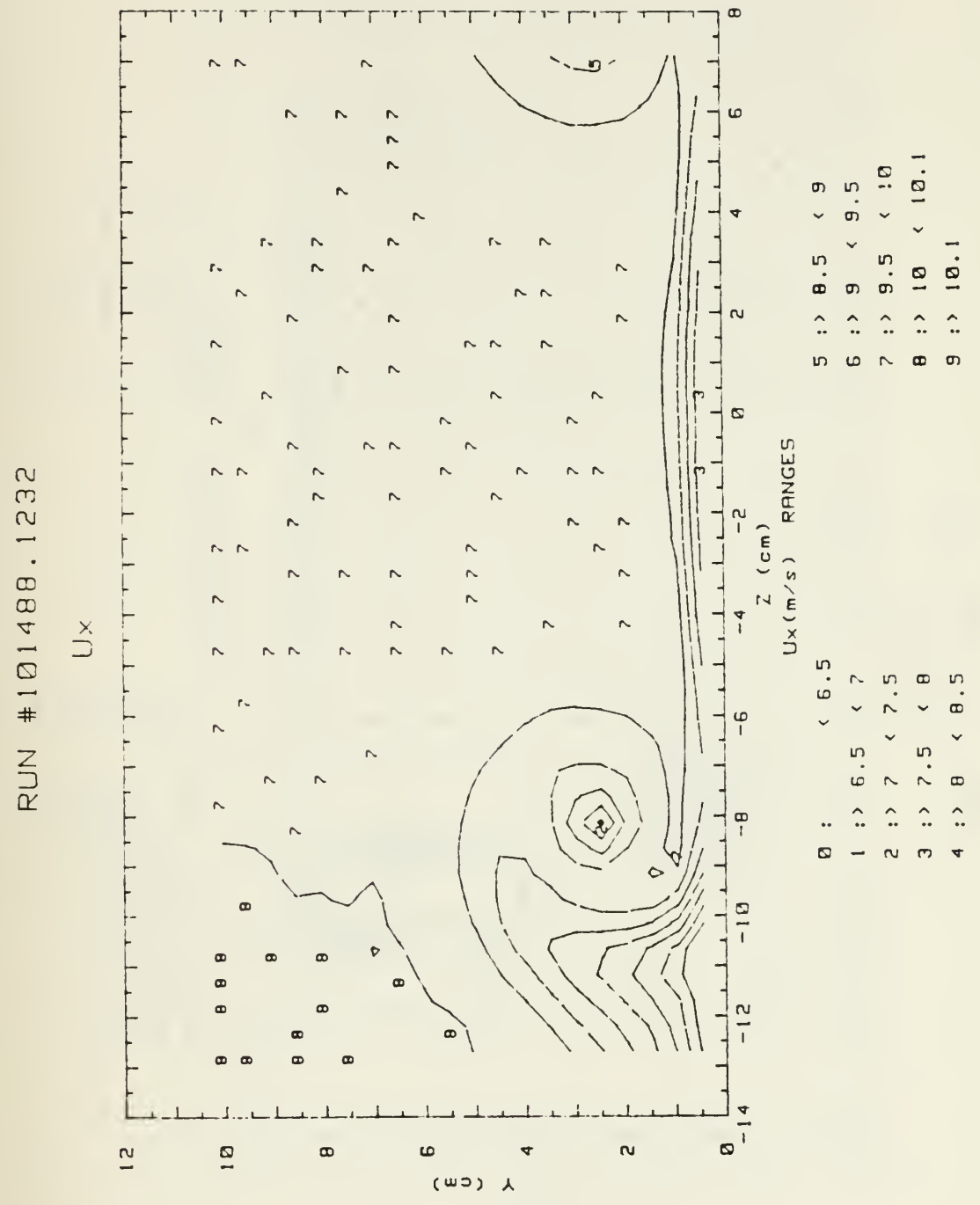

Figure 26. Streamwise Velocity Contours in a Boundary Layer with an Embedded Vortex Pair. b = 7.62 cm, U_∞ = 10 m/s

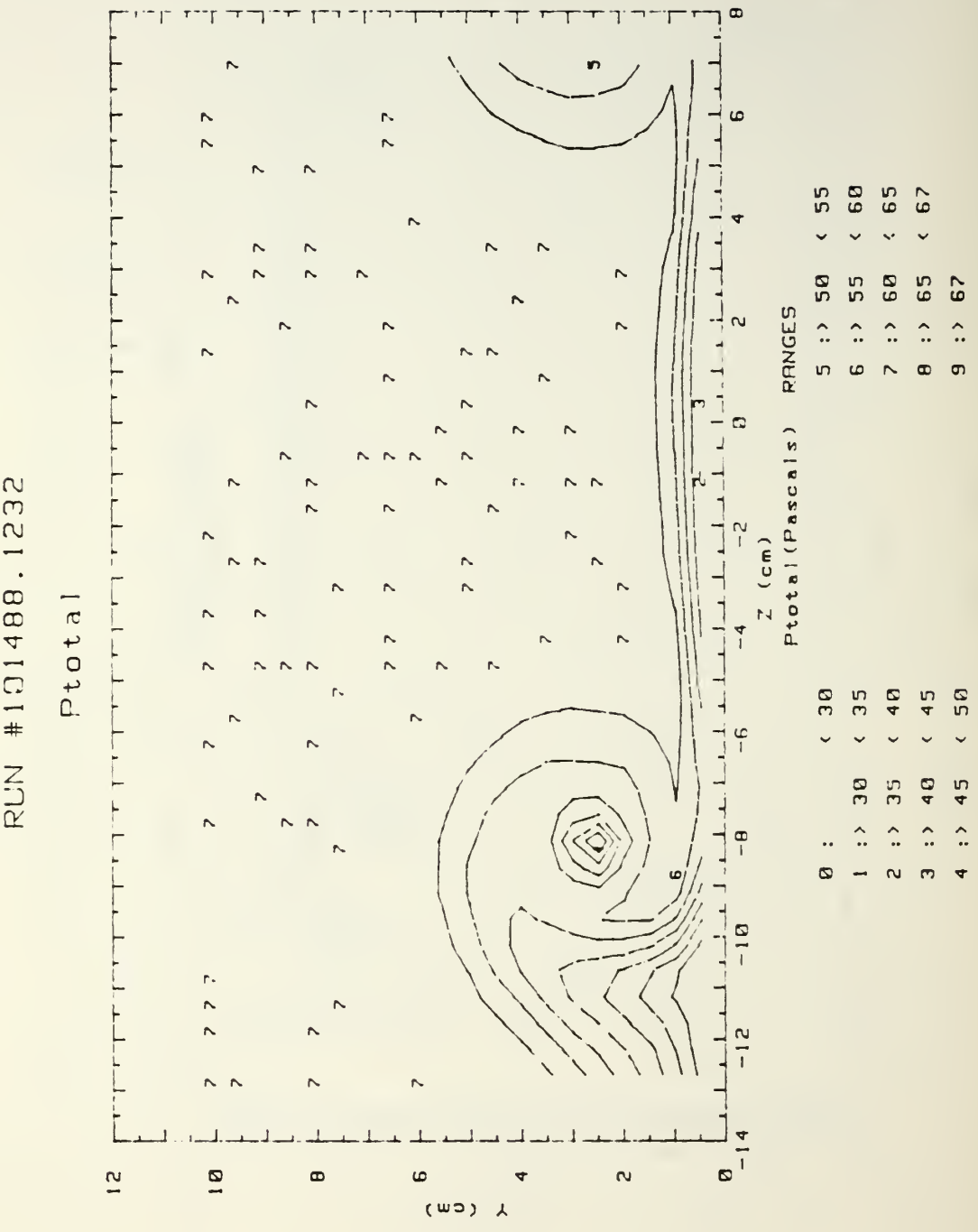

Figure 27. Total Pressure Contours in a Boundary Layer with an Embedded Vortex Pair. b = 7.62 cm, U_∞ = 10 m/s

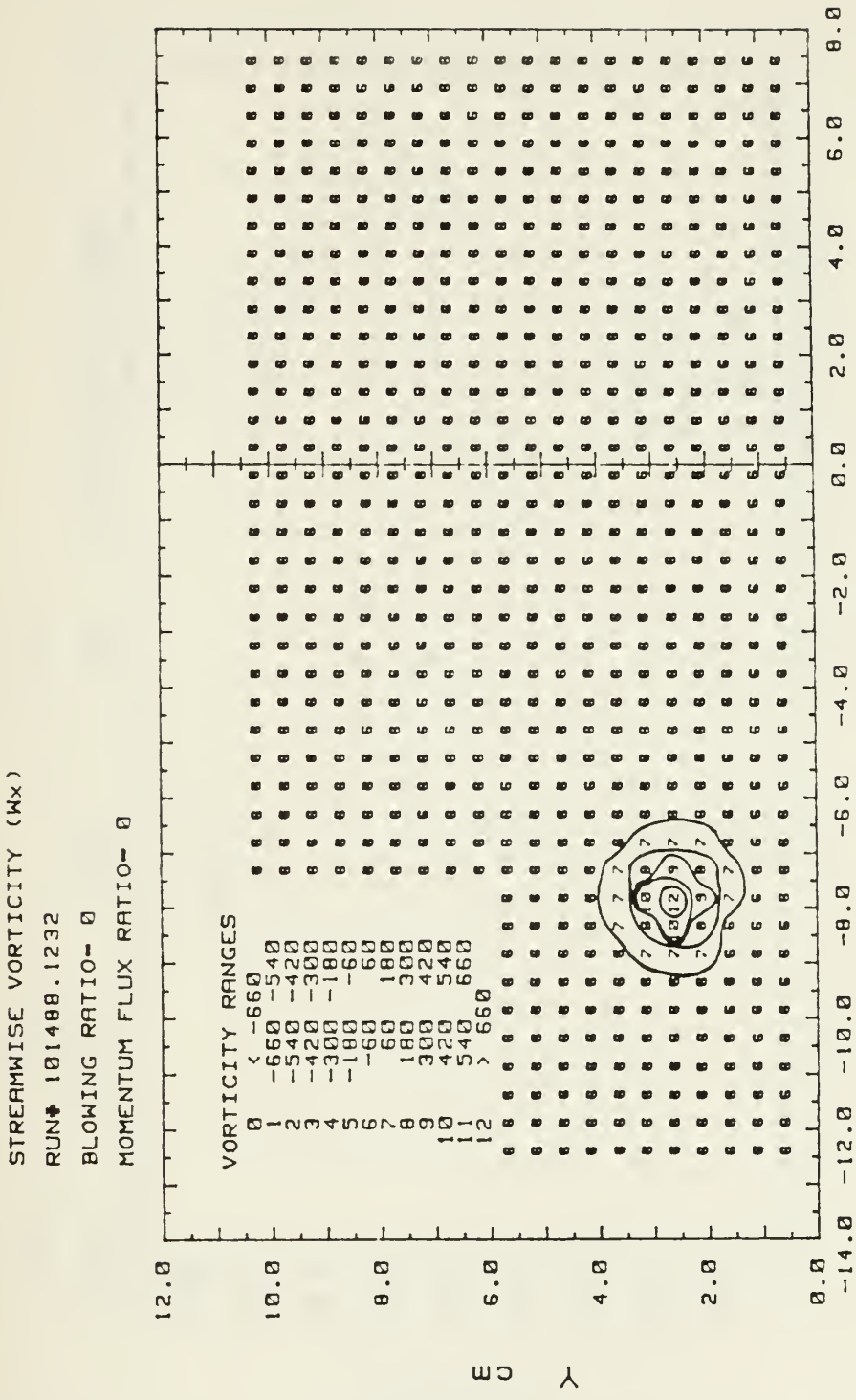

Figure 28. Streamwise Vorticity Contours in a Boundary Layer with an Embedded Vortex Pair.
b = 7.62 cm, U_∞ = 10 m/s

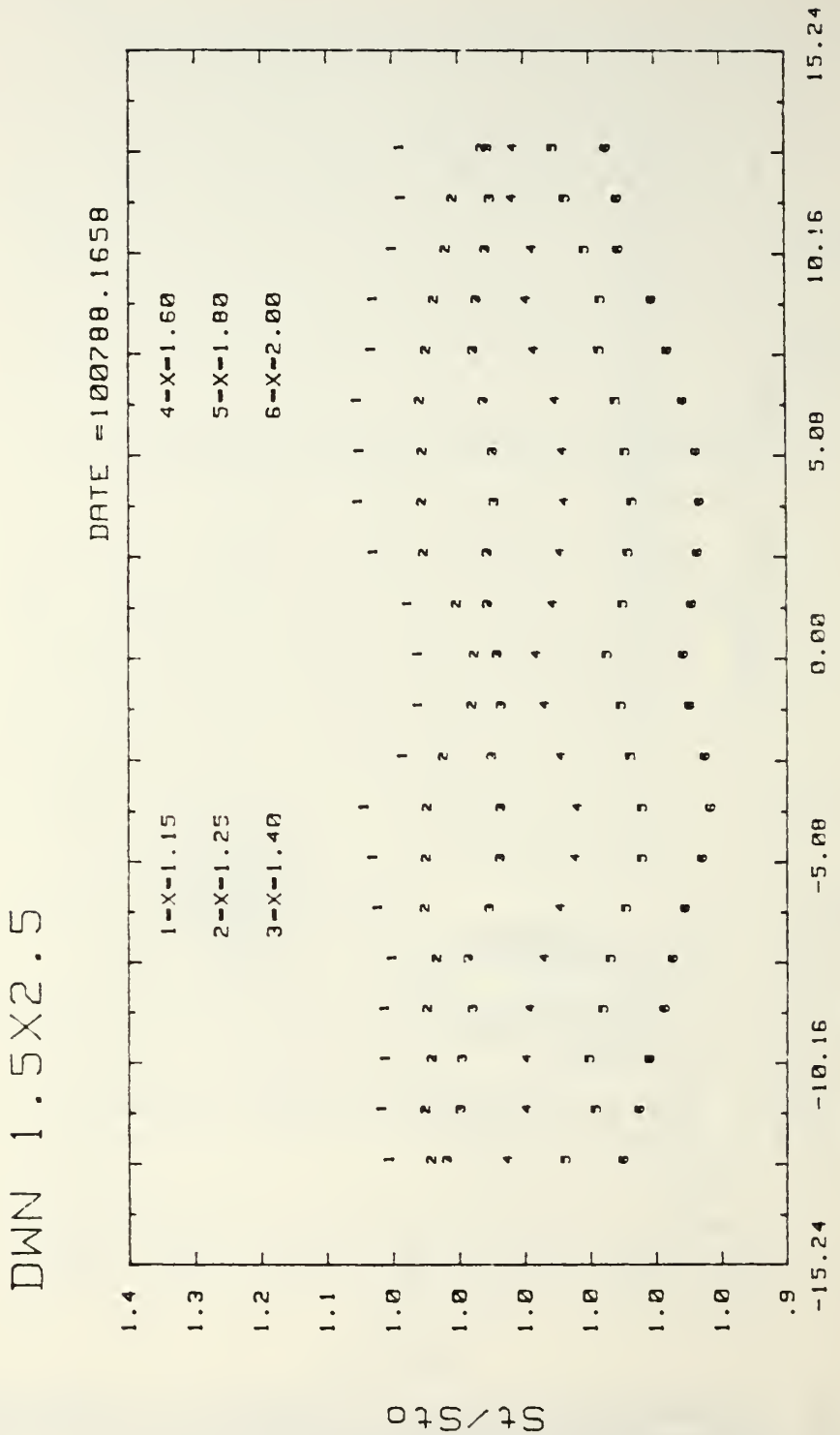

Figure 29. Local St/St_o Ratio Distribution with a Vortex Array in the Downwash Configuration and b = 3.81 cm

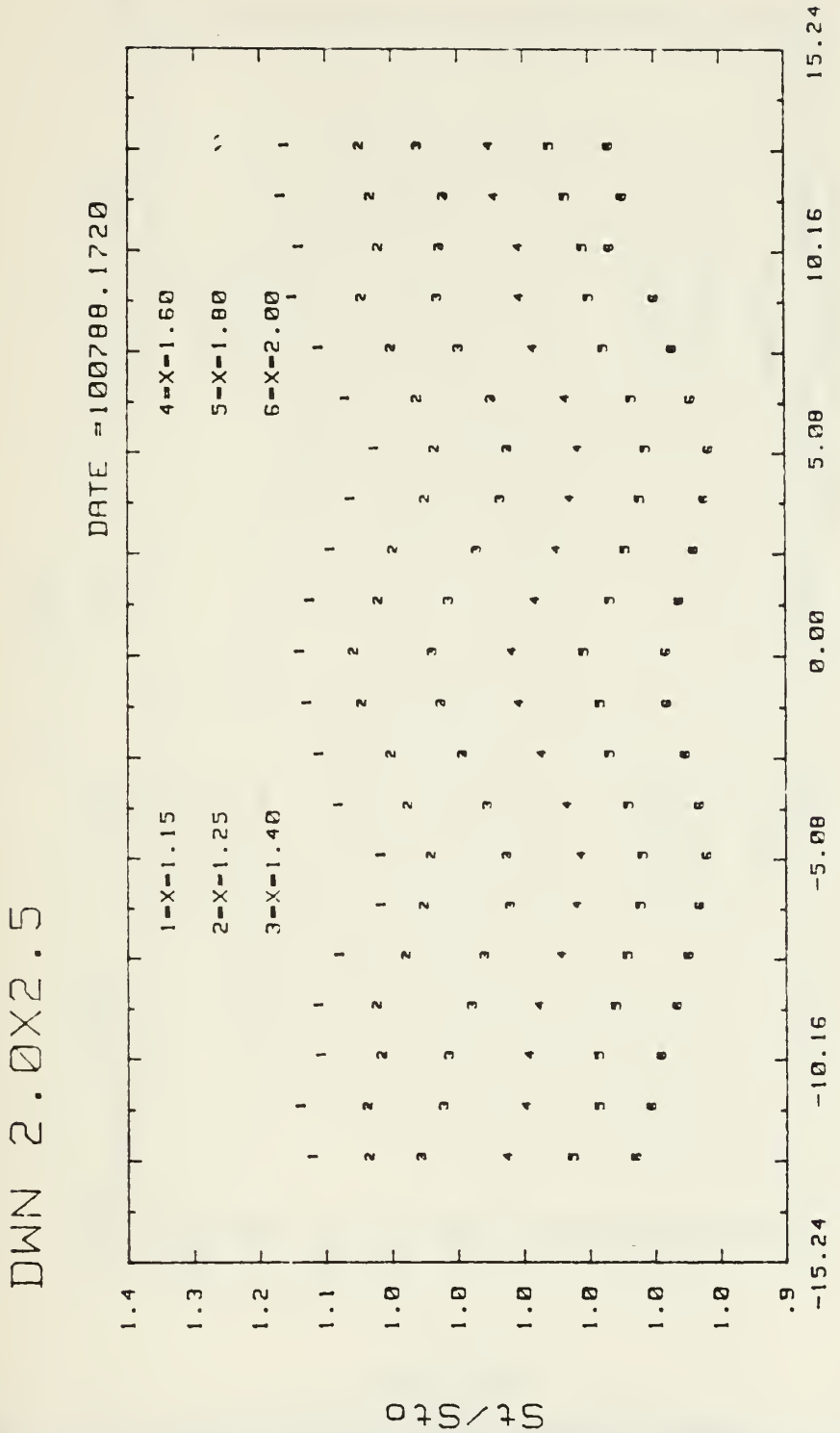

Figure 30. Local St/St_o Ratio Distribution with a Vortex Array in the Downwash Configuration and b = 5.08 cm

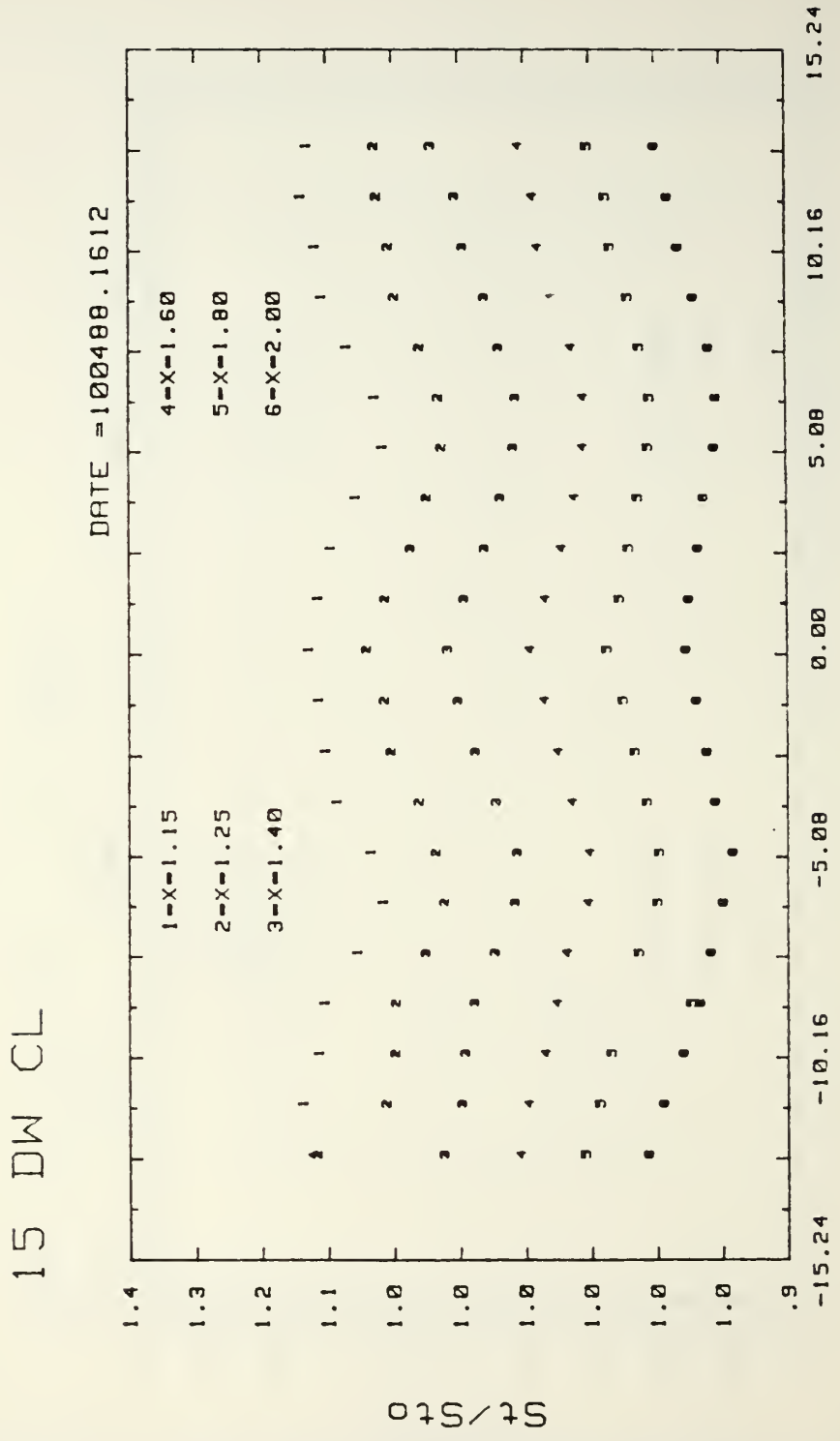

Figure 31. Local St/St_o Ratio Distribution with a Vortex Array in the Downwash Configuration and b = 6.35 cm

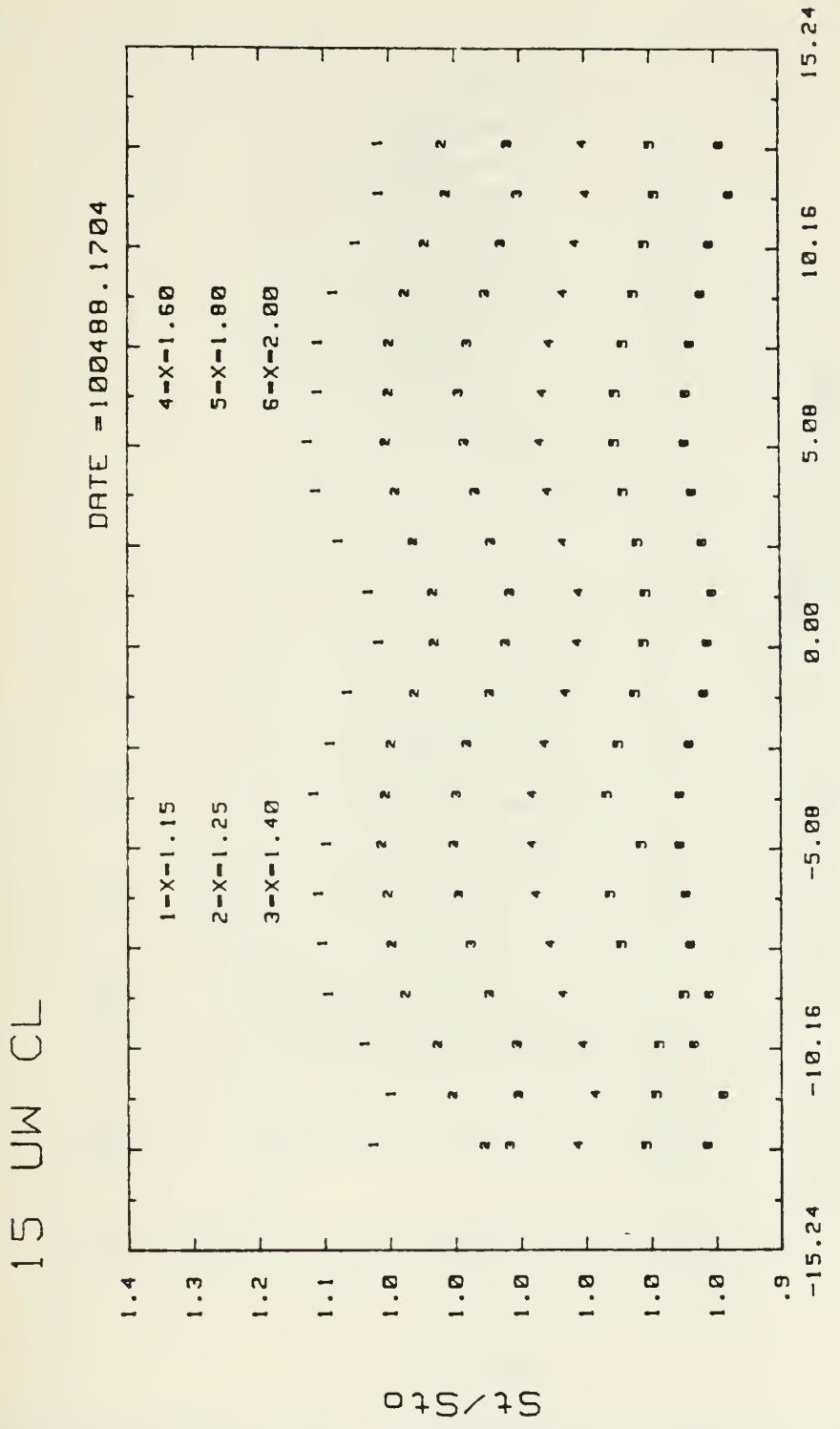

Figure 32. Local St/St_o Ratio Distribution with a Vortex Array in the Downwash Configuration and b = 6.35 cm

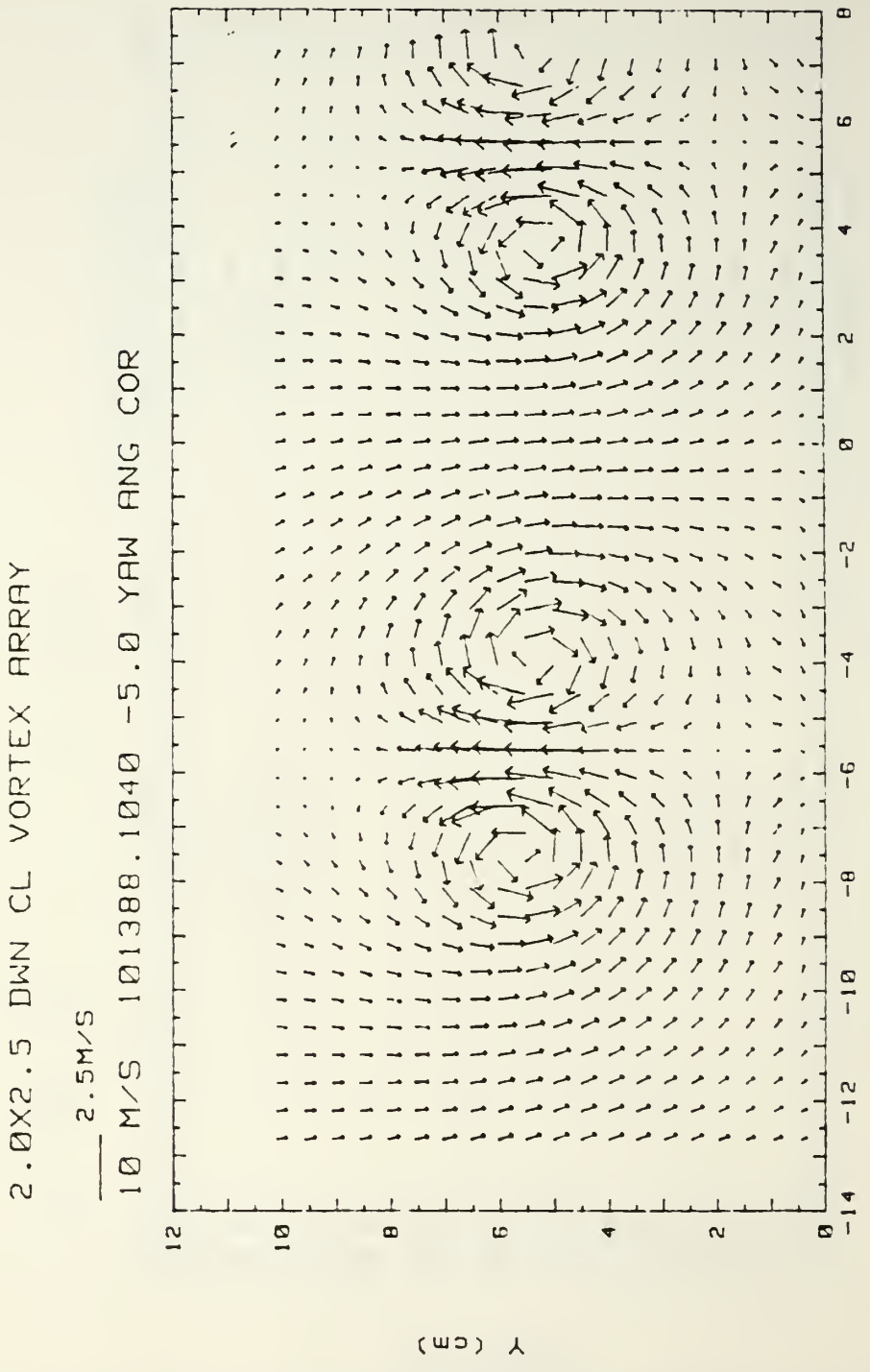

Figure 33. Secondary Flow Vectors in a Boundary Layer with an Embedded Vortex Array. b = 5.08 cm, U_∞ = 10 m/s

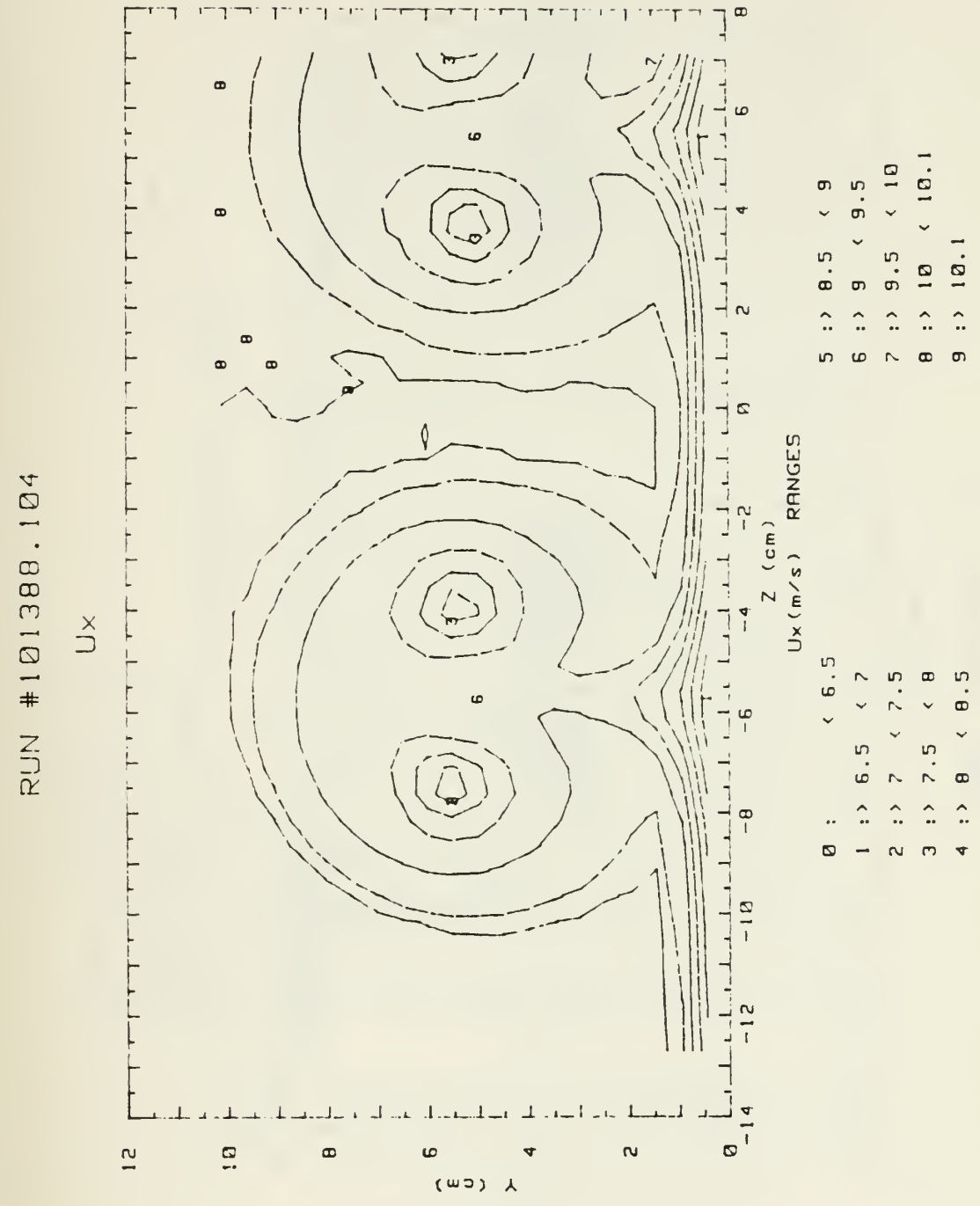

Figure 34. Streamwise Velocity Contours in a Boundary Layer with an Embedded Vortex Array. b = 5.08 cm, U_∞ = 10 m/s

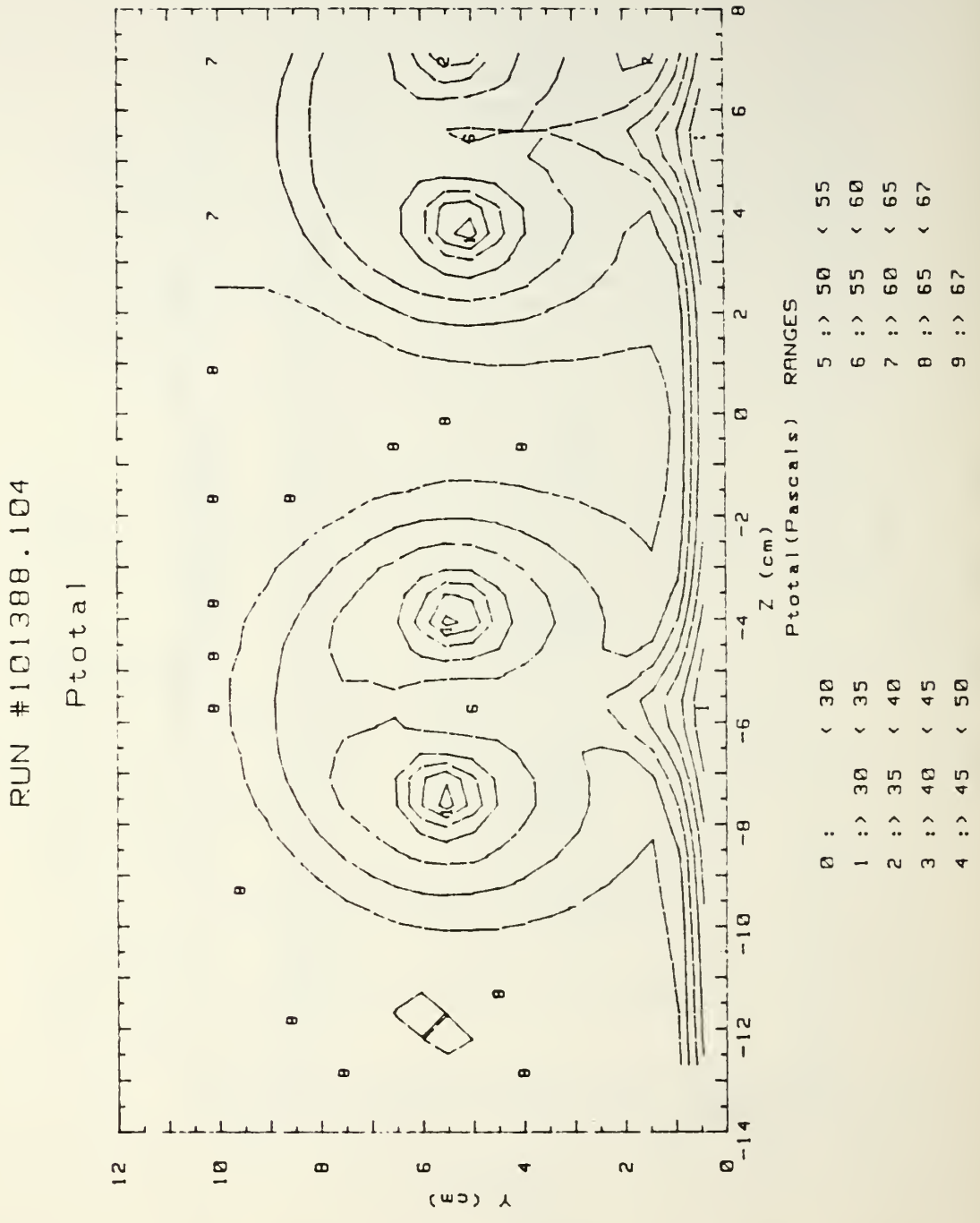

Figure 35. Total Pressure Contours in a Boundary Layer with an Embedded Vortex Array. b = 5.08 cm, U_∞ = 10 m/s

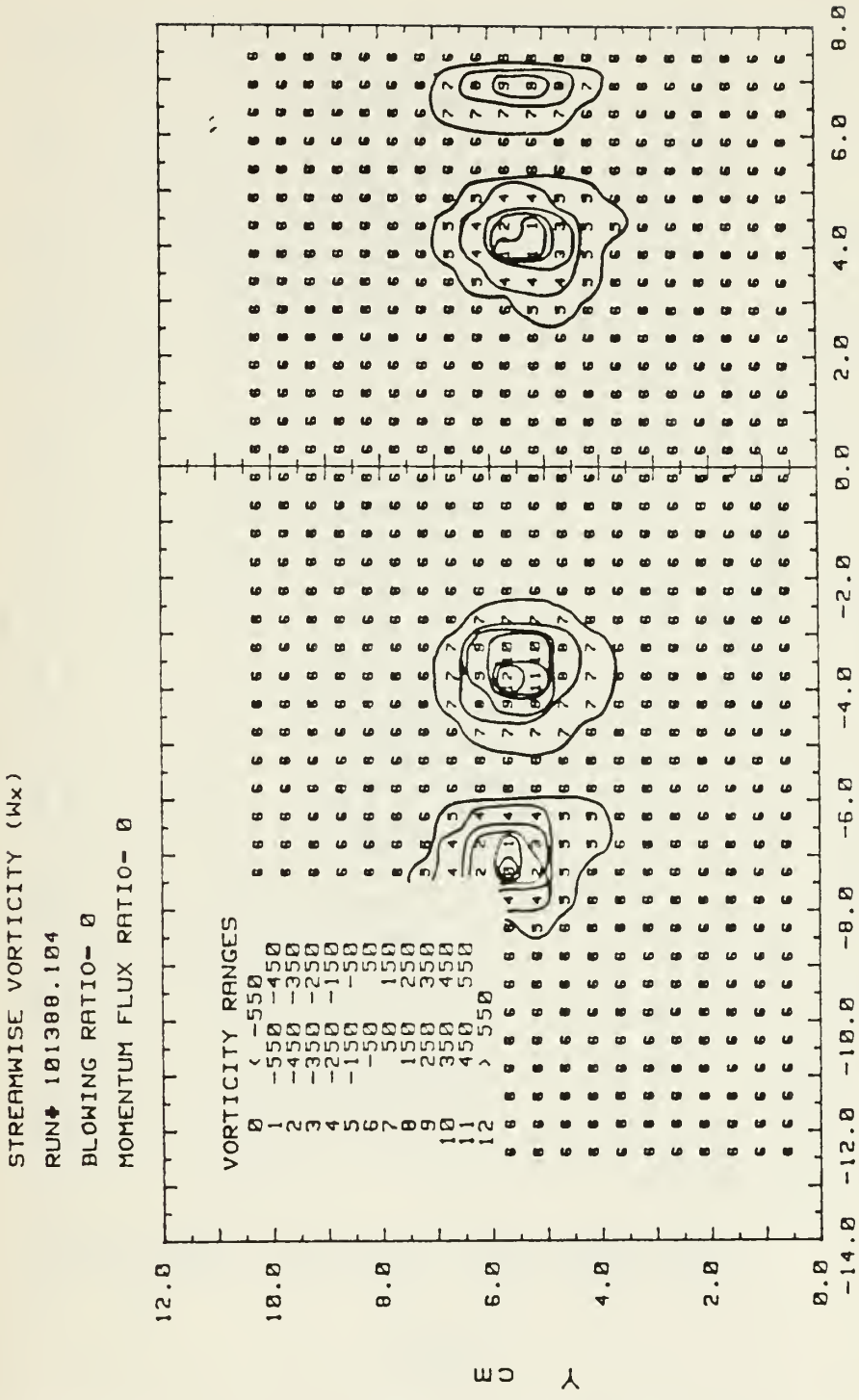

Figure 36. Streamwise Vorticity Contours in a Boundary Layer with an Embedded Vortex Array. b = 5.08 cm, U_∞ = 10 m/s

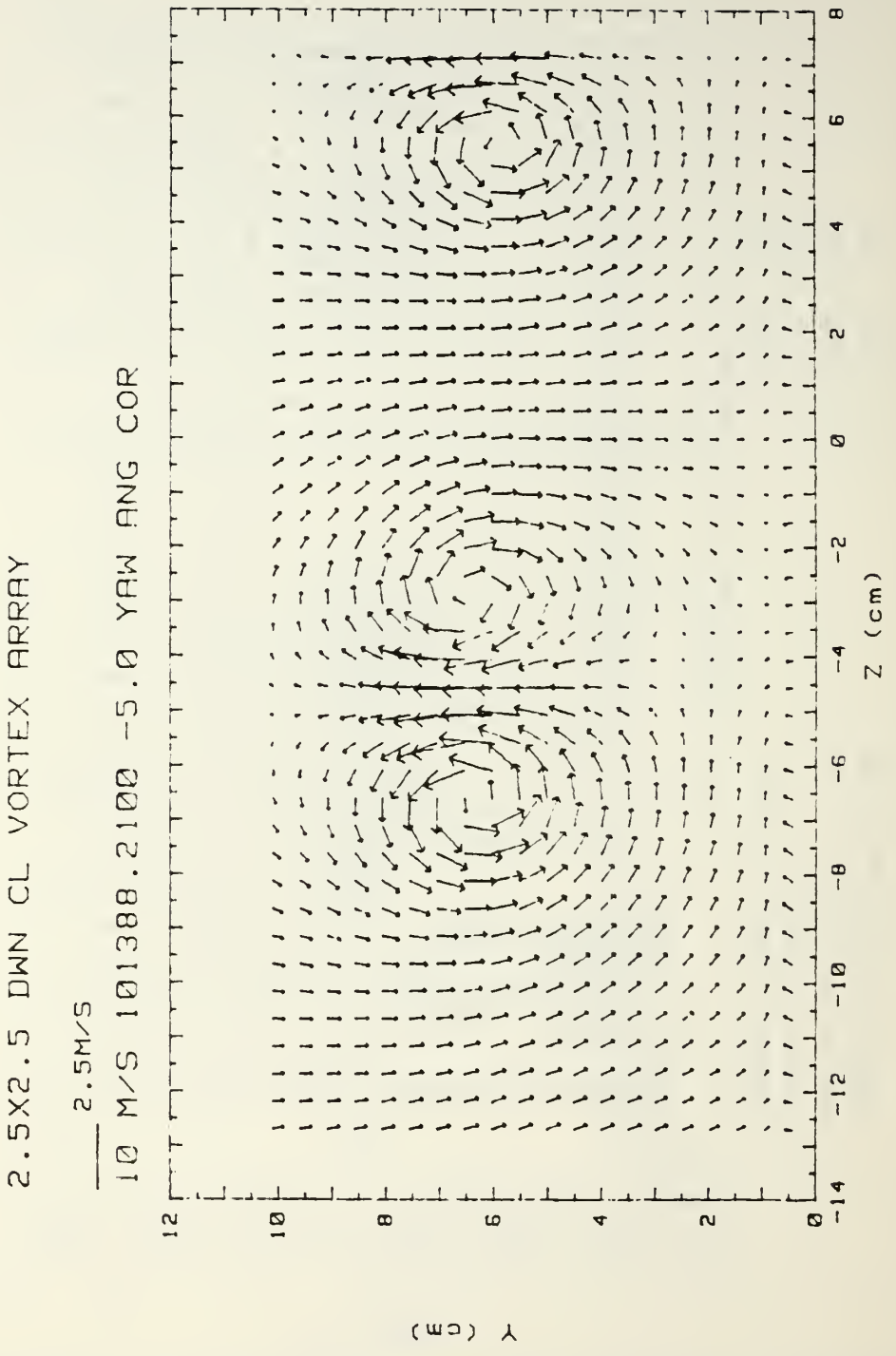

Figure 37. Secondary Flow Vectors in a Boundary Layer with an Embedded Vortex Array. b = 6.35 cm, U_∞ = 10 m/s

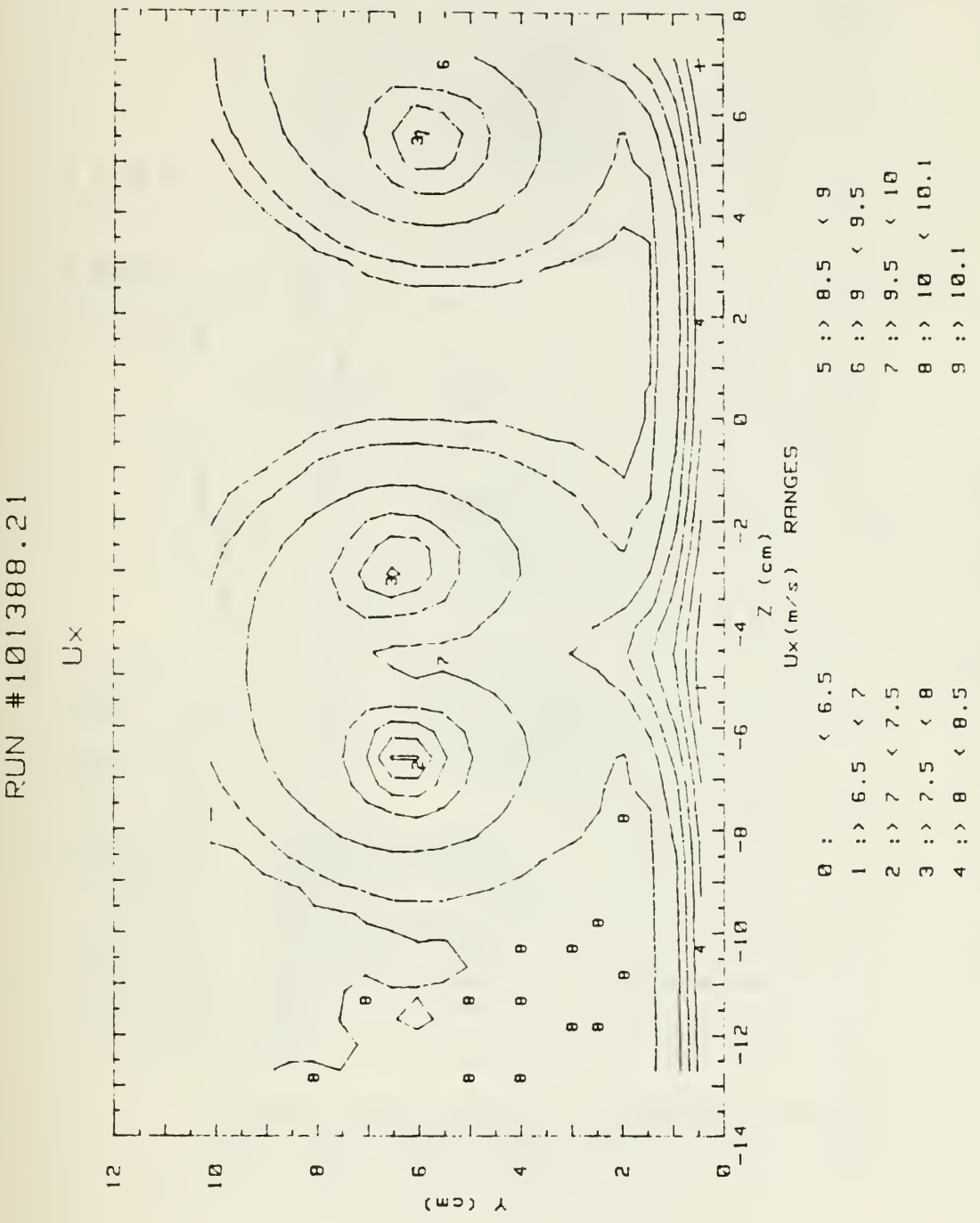

Figure 38. Streamwise Velocity Contours in a Boundary Layer with an Embedded Vortex Array. b = 6.35 cm, U_∞ = 10 m/s

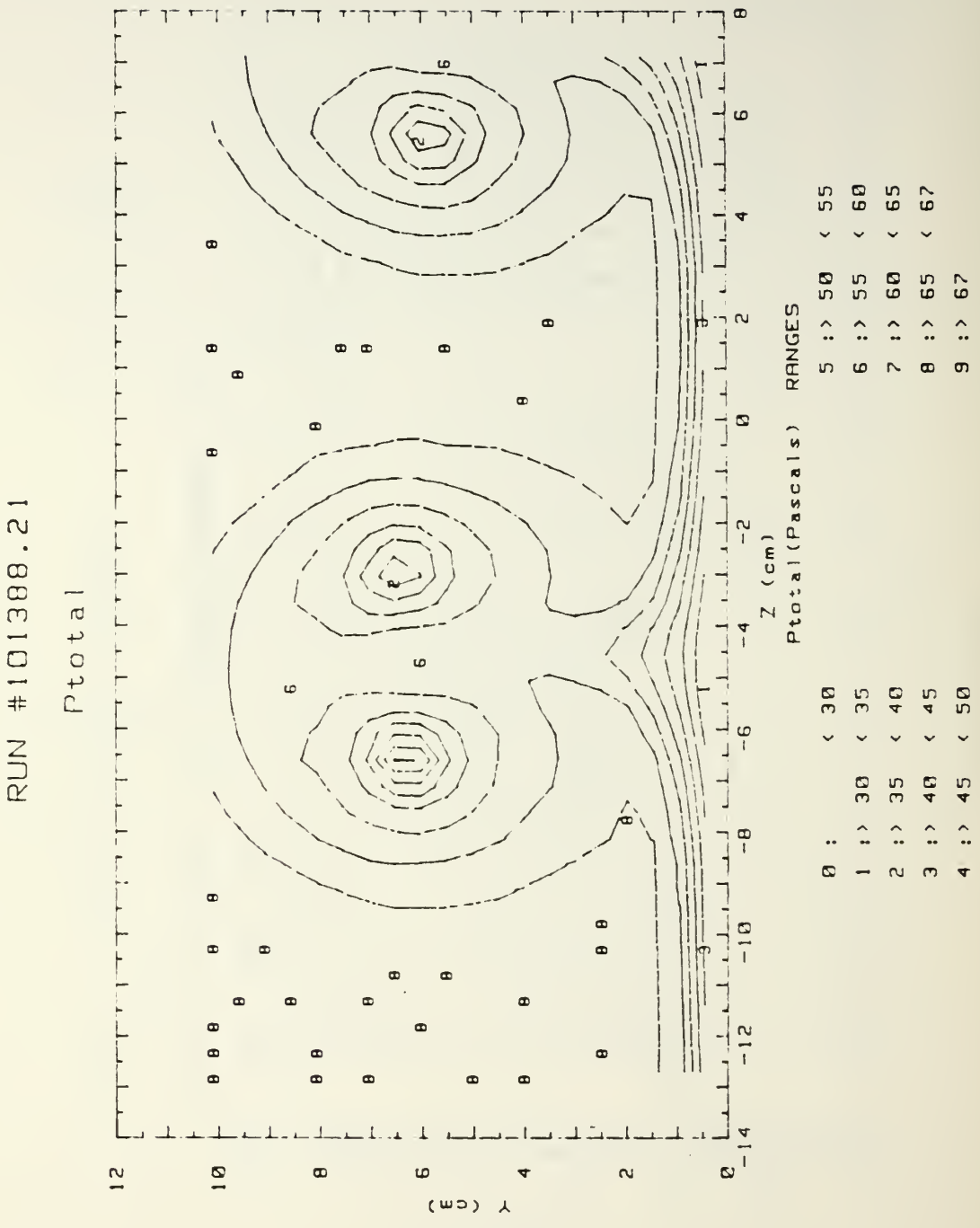

Figure 39. Total Pressure Contours in a Boundary Layer with an Embedded Vortex Array. b = 6.35 cm, U_∞ = 10 m/s

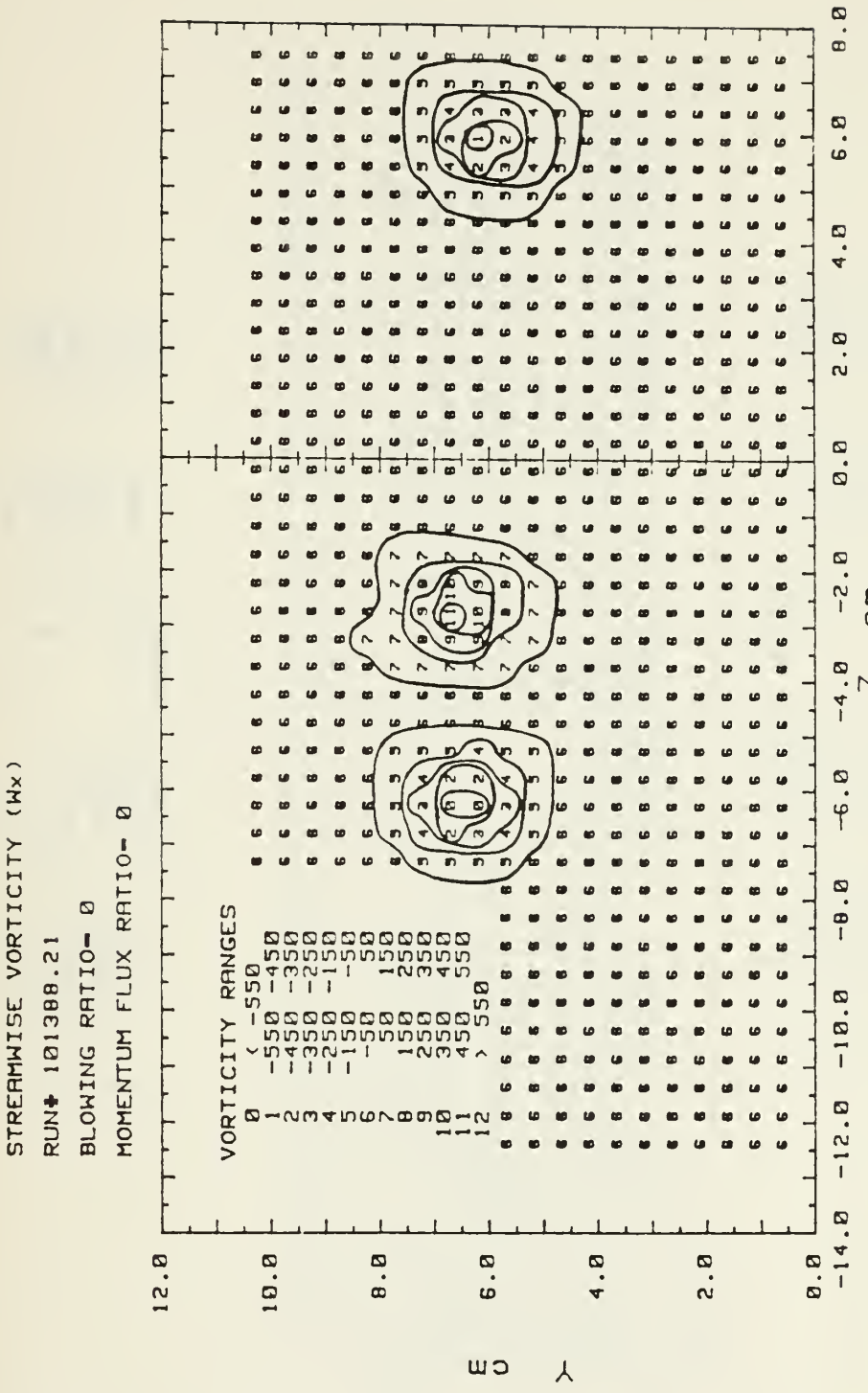

Figure 40. Streamwise Vorticity Contours in a Boundary Layer with an Embedded Vortex Array. b = 6.35 cm, U_∞ = 10 m/s

Figure 41. Streamwise Velocity Contours in a Curved Channel, De = 50

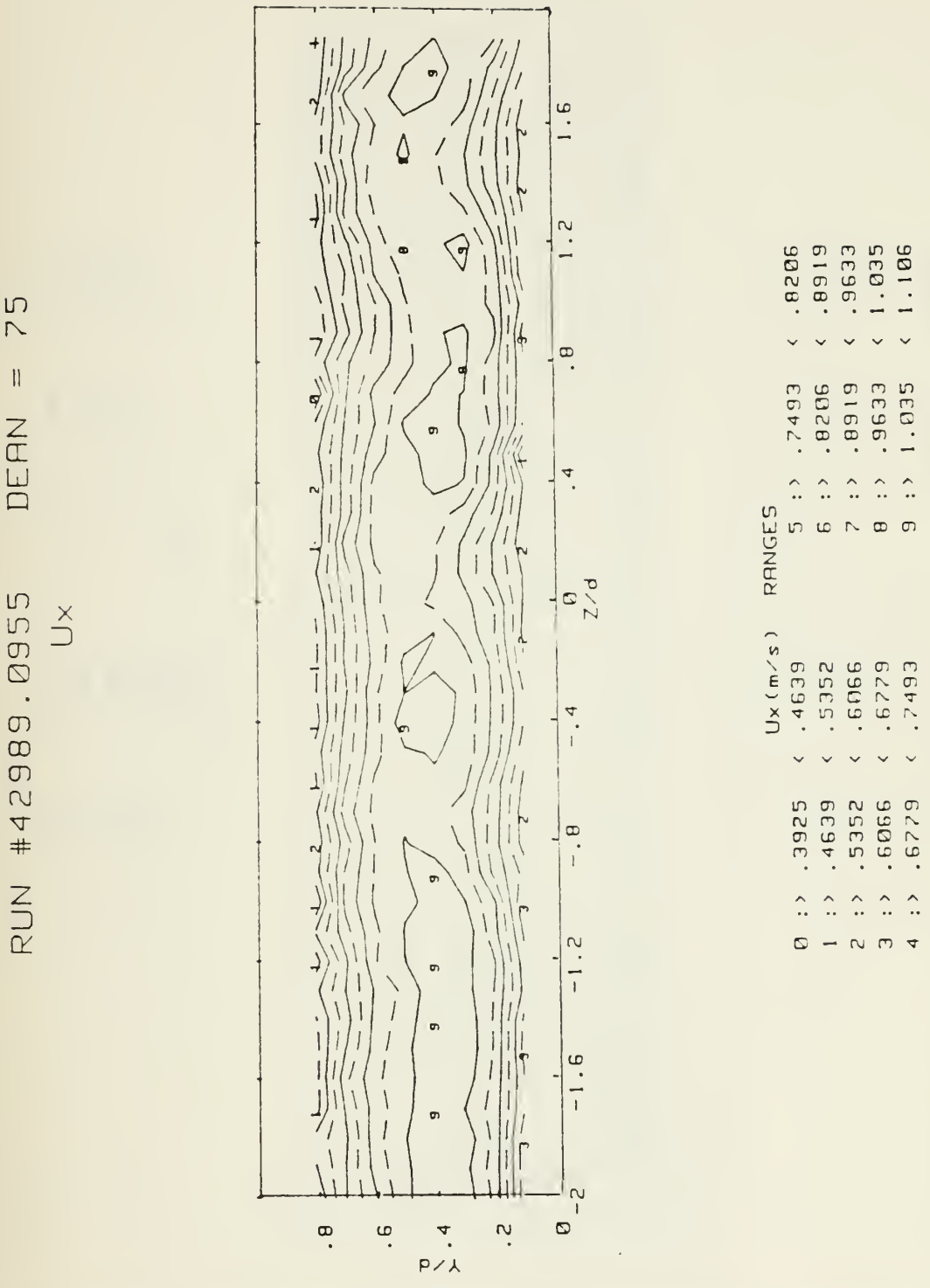

Figure 42. Streamwise Velocity Contours in a Curved Channel, De = 75

Figure 43. Streamwise Velocity Contours in a Curved Channel, De = 100

Figure 44. Streamwise Velocity Contours in a Curved Channel, De = 150

Figure 45. Total Pressure Contours in a Curved Channel, De = 50

Figure 46. Total Pressure Contours in a Curved Channel, De = 75

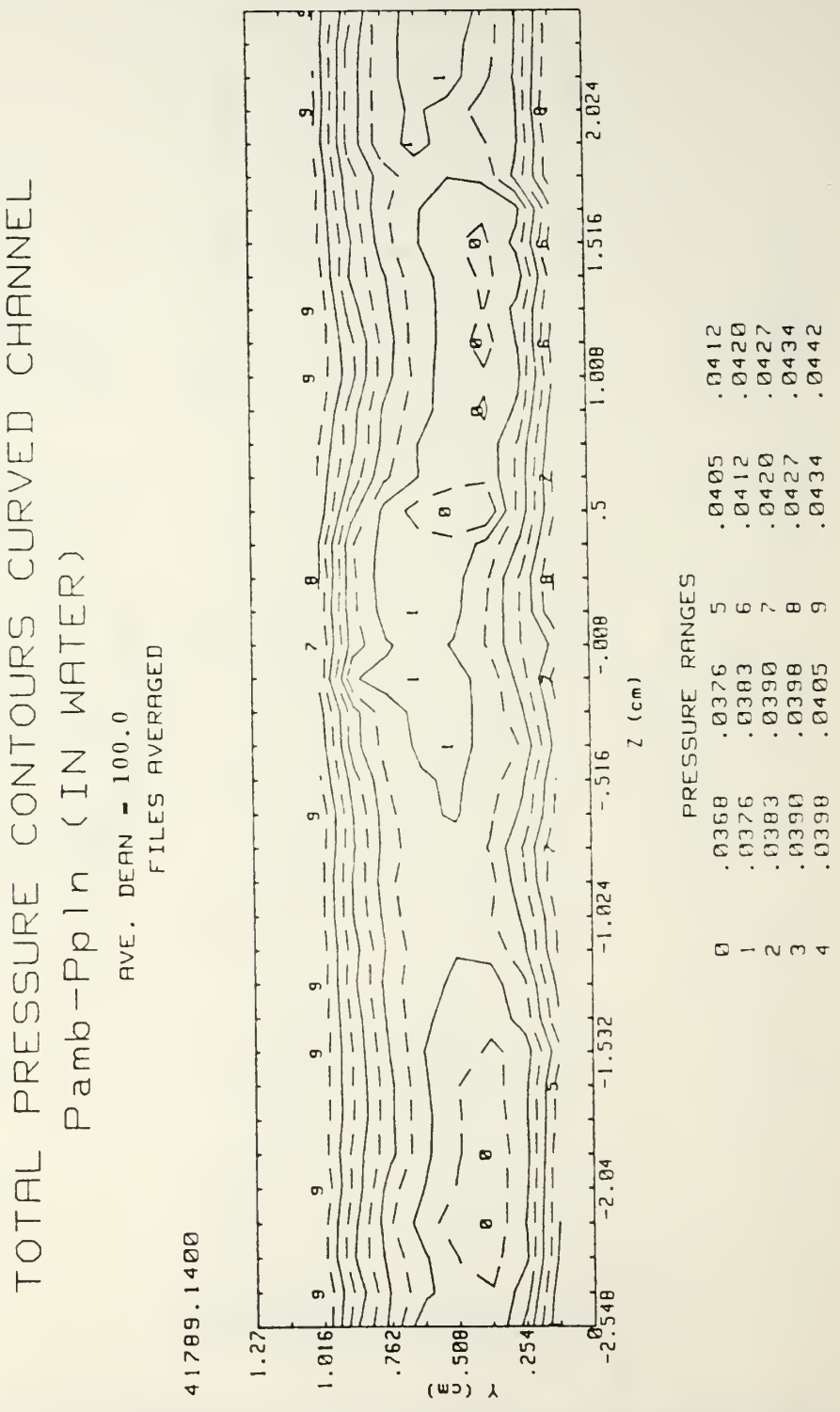

Figure 47. Total Pressure Contours in a Curved Channel, De = 102.7

Figure 48. Total Pressure Contours in a Curved Channel, De = 155.55

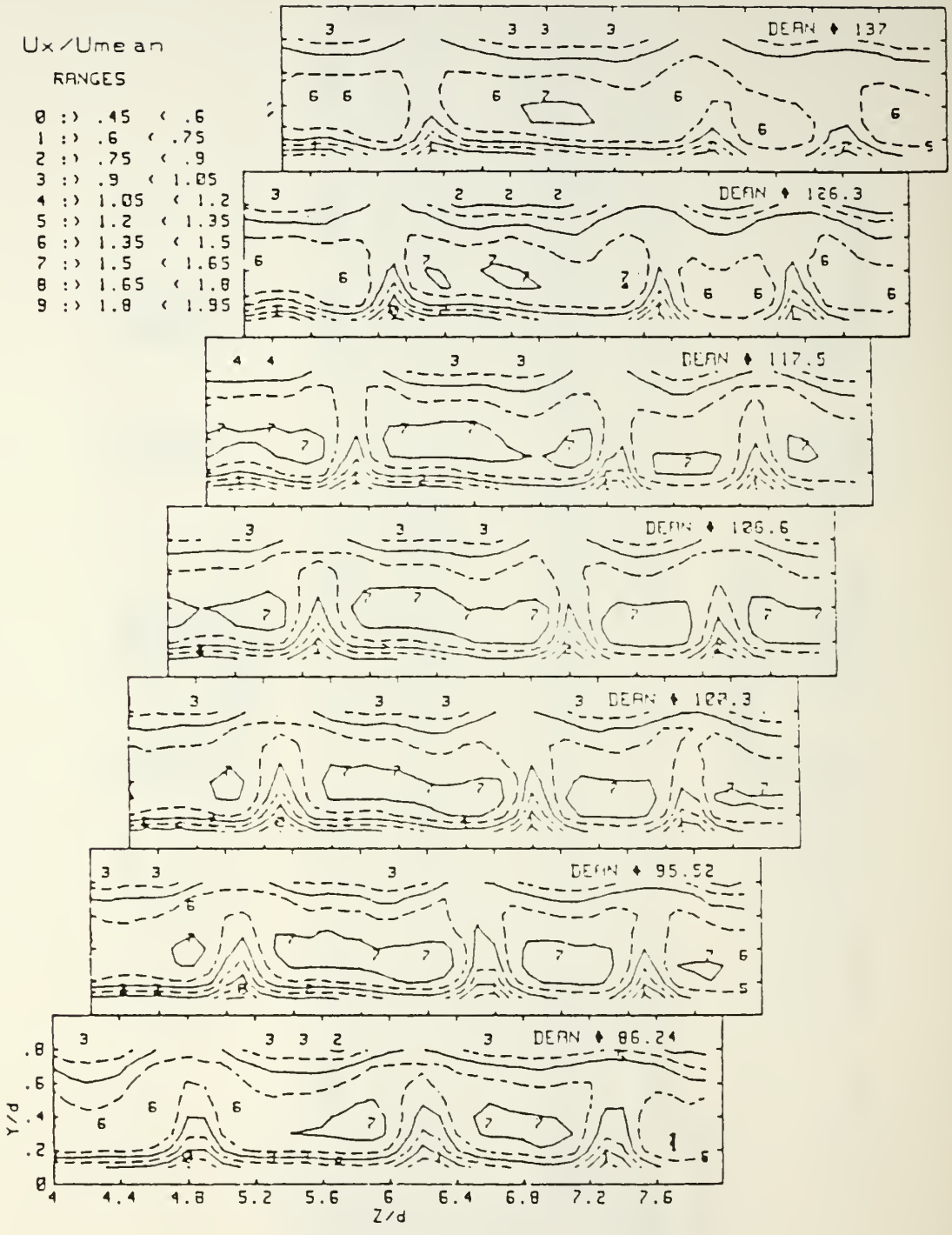

Figure 49. Streamwise Velocity Contours, De = 86.2 to De = 137.0

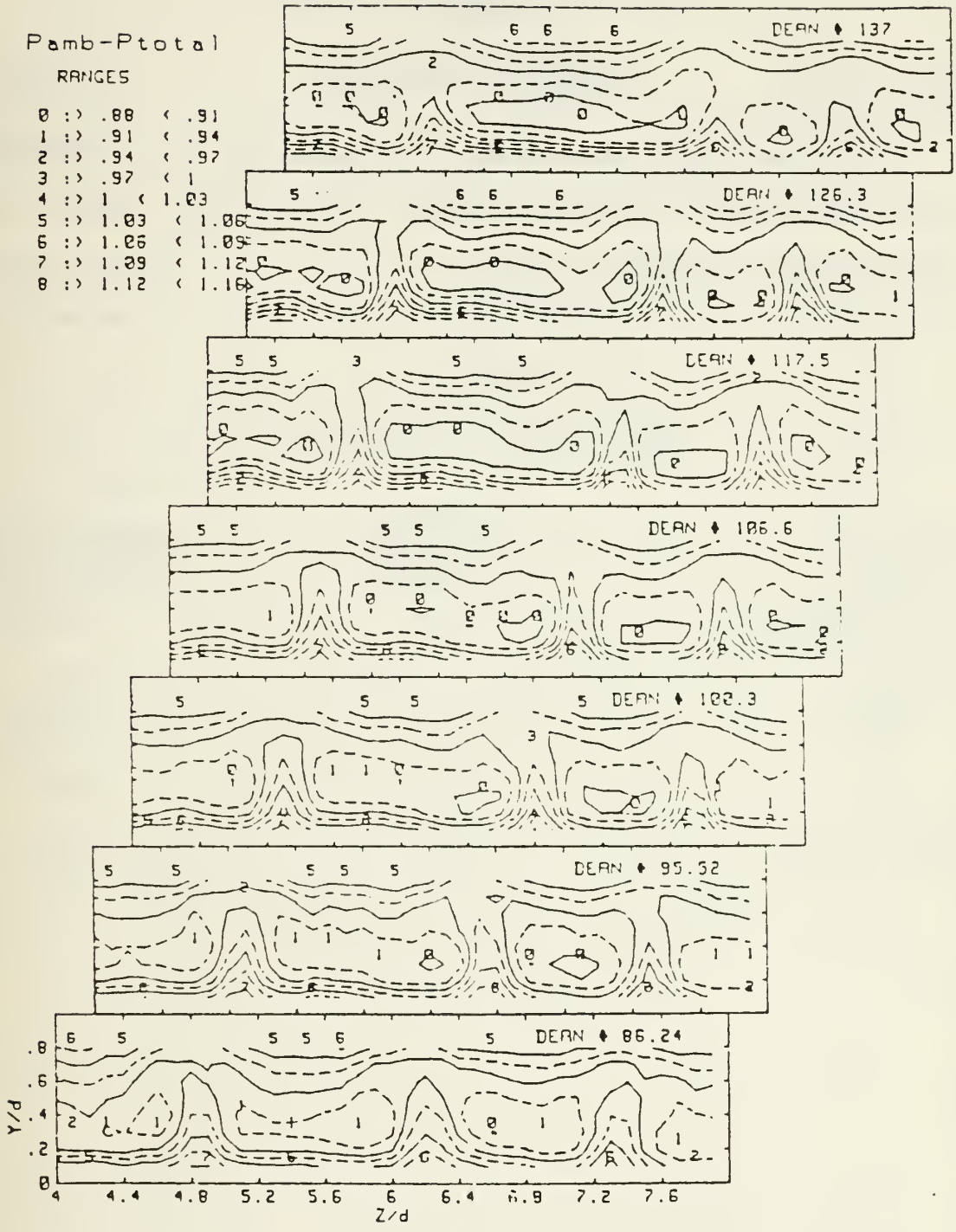

Figure 50. Total Pressure Contours, De = 86.2 to De = 137.0

APPENDIX B

UNCERTAINTY ANALYSIS

For this study, uncertainty estimates for key variables were determined by Schwartz [Ref. 15] and the results are listed below in Tables 1 and 2.

TABLE 1

MEAN VELOCITY UNCERTAINTY

Quantity (Units)	Typical Nominal Value	Experimental Uncertainty
K_y, K_p (units/^{o})	0.09	0.0086
C_{py}, C_{pp}	0.7,0.27	0.02
[illegible] (^{o}C)	10.0	1.2,1.2
U_x (m/s)	10.0	0.25
U_y, U_z (m/s)	1.0	0.09

TABLE 2

STANTON NUMBER UNCERTAINTY

Quantity (Units)	Typical Nominal Value	Experimental Uncertainty
Tr_∞ (^oC)	18.0	0.13
T_W (^oC)	40.0	0.21
P_{amb} (mm Hg)	760.0	0.71
P_∞ (mm Hg)	760.0	0.71
$(Po_\infty - P_\infty)$ (mm H_2O)	6.13	0.047
P_∞ (kg/m^3)	1.23	0.009
U_∞, U_x (m/s)	10.0	0.06
C_p ($J/kg \cdot {}^oK$)	1006.0	1.0
$q_W A$ (W)	270.0	10.5
St	0.00196	0.000086
St/St_o	1.05	0.058

LIST OF REFERENCES

1. Ligrani, P.M., Joseph, S.L, Ortiz, A., and Evans, D.L., "Heat Transfer in Film-Cooled Turbulent Boundary Layers at Different Blowing Ratios as Affected by Longitudinal Vortices," Experimental Thermal and Fluid Science, Vol. 1, No. 4, pp. 347-362, 1988.

2. Eibeck, P.A., and Eaton, J.K., "Heat Transfer Effects of a Longitudinal Vortex Embedded in a Turbulent Boundary Layer," ASME Transactions--Journal of Heat Transfer, Vol. 104, pp. 355-362, 1987.

3. Ligrani, P.M., Ortiz, A., Joseph, S.L., and Evans, D.L., "Effects of Embedded Vortices on Film-Cooled Turbulent Boundary Layers," ASME Paper No. 88-GT-170, ASME Gas Turbine and Aeroengine Congress and Exposition, Amsterdam, The Netherlands, June 1988, also, ASME Transactions--Journal of Turbomachinery, Vol. 111, pp. 71-77, 1989.

4. Ligrani, P.M. and Williams, W., "Effects of an Embedded Vortex on Injectant from a Single Film-Cooling Hole in a Turbulent Boundary Layer," ASME Paper No. 89-GT-189, pp. 1-11, ASME Gas Turbine and Aeroengine Congress and Exposition, Toronto, Ontario, Canada, June, 1989, also to appear in ASME Transactions--Journal of Turbomachinery, January 1990.

5. Craig, D.W., Effects of Vortex Circulation on Injectant from a Single Film-Cooling Hole and a Row of Film-Cooling Holes in a Turbulent Boundary Layer, Part 1: Injection Beneath the Vortex Downwash, Master's Thesis, Naval Postgraduate School, Monterey, California, June 1989.

6. Westphal, R.V., Pauley, W.R., and Eaton, J.K., "Interaction Between a Vortex and a Turbulent Boundary Layer, Part I: Mean Flow Evolution and Turbulence Properties," NASA Technical Memorandum 88361, January 1987.

7. Westphal, R.V., Eaton, J.K., and Pauley, W.R., "Interaction Between a Vortex and a Turbulent Boundary Layer in a Streamwise Pressure Gradient," 5th Symposium on Turbulent Shear Flows, Cornell University, Ithaca, New York, 1985.

8. Wang, T., An Investigation of Curvature and Free Stream Turbulence Effects on Heat Transfer and Fluid Mechanics in Transitional Boundary Layer Flows, Ph.D. Thesis, Mechanical Engineering Department, University of Minnesota, December 1984.

9. Wang, T., Simon, W.T., and Buddhavarapin, J., "Heat Transfer and Fluid Mechanics Measurements in Transitional Boundary Layer Flows," Gas Turbine Division of American Society of Mechanical Engineers, ASME Paper No. 85-GT-113, pp. 1-9, 1985.

10. Ortiz, A., The Thermal Behavior of Film Cooled Turbulent Boundary Layers as Affected by Longitudinal Vortices, Master's Thesis, Naval Postgraduate School, Monterey, California, September 1987.

11. Joseph, S.L., The Effects of an Embedded Vortex on a Film Cooled Turbulent Boundary Layer, Master's Thesis, Naval Postgraduate School, Monterey, California, December 1986.

12. Williams, W., Effects of an Embedded Vortex on a Single Film-Cooling Jet in a Turbulent Boundary Layer, Master's Thesis, Naval Postgraduate School, Monterey, California, June 1988.

13. Kays, W.M., and Crawford, M.E., Convective Heat and Mass Transfer, Second Edition, p. 216, McGraw-Hill Book Company, 1980.

14. Baun, L.R., The Development and Structural Characteristics of Dean Vortices in a Curved Rectangular Channel with 40 to 1 Aspect Ratio, Master's Thesis, Naval Postgraduate School, Monterey, California, September 1988.

15. Schwartz, G.E., Control of Embedded Vortices Using Wall Jets, Master's Thesis, Naval Postgraduate School, Monterey, California, September 1988.

INITIAL DISTRIBUTION LIST

		No. Copies
1.	Defense Technical Information Center Cameron Station Alexandria, Virginia 22304-6145	2
2.	Library, Code 0142 Naval Postgraduate School Monterey, California 93943-5002	2
3.	Department Chairman, Code 69 Department of Mechanical Engineering Naval Postgraduate School Monterey, California 93943-5000	1
4.	Professor Phillip M. Ligrani, Code 69Li Department of Mechanical Engineering Naval Postgraduate School Monterey, California 93943-5000	10
5.	LT Michael F. Tuzzolo, USN 266 Sanilac Street Staten Island, New York 10306	2
6.	Professor Chelakara S. Subramanian, Code 69Su Department of Mechanical Engineering Naval Postgraduate School Monterey, California 93943-5000	2

Thesis
T9588
c.2

Tuzzolo
Study of vortex arrays induced artificially and from centrifugal instabilities.